Since January 2020 Elsevier has created a COVID-19 resource centre with free information in English and Mandarin on the novel coronavirus COVID-19. The COVID-19 resource centre is hosted on Elsevier Connect, the company's public news and information website.

European Journal of Medicinal Chemistry 226 (2021) 113863

Contents lists available at ScienceDirect

European Journal of Medicinal Chemistry

journal homepage: http://www.elsevier.com/locate/ejmech

Identification of a dual acting SARS-CoV-2 proteases inhibitor through in silico design and step-by-step biological characterization

Veronica Di Sarno [a, 1], Gianluigi Lauro [a, 1], Simona Musella [b], Tania Ciaglia [a], Vincenzo Vestuto [a], Marina Sala [a], Maria Carmina Scala [a], Gerardina Smaldone [a], Francesca Di Matteo [a], Sara Novi [a], Mario Felice Tecce [a], Ornella Moltedo [a], Giuseppe Bifulco [a], Pietro Campiglia [a, b], Isabel M. Gomez-Monterrey [c], Robert Snoeck [d], Graciela Andrei [d], Carmine Ostacolo [c, *], Alessia Bertamino [a, **]

[a] Department of Pharmacy, University of Salerno, Via G. Paolo II 132, 84084, Fisciano, Salerno, Italy
[b] European Biomedical Research Institute (EBRIS), Via S. De Renzi 50, 84125, Salerno, Italy
[c] Department of Pharmacy, University Federico II of Naples, Via D. Montesano 49, 80131, Naples, Italy
[d] Rega Institute for Medical Research, Department of Microbiology, Immunology, and Transplantation, KU Leuven, BE-3000, Leuven, Belgium

ARTICLE INFO

Article history:
Received 22 July 2021
Received in revised form
17 September 2021
Accepted 18 September 2021
Available online 22 September 2021

Keywords:
In-silico design
SARS-CoV-2 proteases dual inhibitor
Enzymatic assays
Biophysical assays
Cellular characterization

ABSTRACT

COVID-19 pandemic, starting from the latest 2019, and caused by SARS-CoV-2 pathogen, led to the hardest health-socio-economic disaster in the last century. Despite the tremendous scientific efforts, mainly focused on the development of vaccines, identification of potent and efficient anti-SARS-CoV-2 therapeutics still represents an unmet need. Remdesivir, an anti-Ebola drug selected from a repurposing campaign, is the only drug approved, so far, for the treatment of the infection. Nevertheless, WHO in later 2020 has recommended against its use in COVID-19. In the present paper, we describe a step-by-step in silico design of a small library of compounds as main protease (M^{pro}) inhibitors. All the molecules were screened by an enzymatic assay on M^{pro} and, then, cellular activity was evaluated using Vero cells viral infection model. The cellular screening disclosed compounds **29** and **34** as in-vitro SARS-CoV-2 replication inhibitors at non-toxic concentrations ($0.32 < EC_{50} < 5.98$ μM). To rationalize these results, additional in-vitro assays were performed, focusing on papain like protease (PL^{pro}) and spike protein (SP) as potential targets for the synthesized molecules. This pharmacological workflow allowed the identification of compound **29**, as a dual acting SARS-CoV-2 proteases inhibitor featuring micromolar inhibitory potency versus M^{pro} ($IC_{50} = 1.72$ μM) and submicromolar potency versus PL^{pro} ($IC_{50} = 0.67$ μM), and of compound **34** as a selective SP inhibitor ($IC_{50} = 3.26$ μM).

1. Introduction

SARS-CoV-2 (severe acute respiratory syndrome coronavirus 2) is the pathogen causing Coronavirus disease 2019 (COVID-19). SARS-CoV-2 belongs to the β-coronaviridae family of which bats represent the main reservoir and many proofs suggest that human infection was a result of a zoonotic jump [1,2].

The first evidence of this pathology was recognized in Wuhan, China in the late 2019 and since this date SARS-CoV-2 has caused a worldwide outbreak as declared by WHO in March 2020. Up to now, more than 150 million of cases with about 3 million of deaths have been associated with this pathology in the whole world. The pandemic is still in progress, causing not only the hardest sanitary crisis in the last century, but also an unrecoverable socio-economic collapse. COVID-19 symptoms can range from very mild to severe and include fever, cough, tiredness and loss of taste and smell, but the infection can degenerate, spreading deeply into lungs and causing bilateral pneumonia as principal cause of death, especially in frail elderly patients [3,4].

Despite all the efforts, during the last year, addressed to build an efficient vaccine campaign, the virus spread is still ongoing and the challenge is still open. For these reasons, the main action to fight

* Corresponding author.
** Corresponding author.
E-mail addresses: ostacolo@unina.it (C. Ostacolo), abertamino@unisa.it (A. Bertamino).
[1] These authors contributed equally to this work.

https://doi.org/10.1016/j.ejmech.2021.113863
0223-5234/

this global pandemic is based on breaking the transmission chain of SARS-CoV-2, facing not only the high infectiousness [5], but also the mutations rate, that leads to a large number of unknown, perhaps vaccine-resistant strains [6]. A proper pharmacological therapy is not currently yet available for COVID-19. Remdesivir, an RNA-dependent RNA-polymerase inhibitor developed in 2014 as anti-Ebola drug, represents the only antiviral drug approved by the FDA for the treatment of hospitalized patients with COVID-19 [7]. Nevertheless, in late 2020, WHO has issued a conditional recommendation against the use of remdesivir in hospitalized patients, as no evidences were collected concerning remdesivir improvement in survival and other outcomes in these patients [8]. Drug repurposing, in fact, is the most used approach to set up an appropriate therapy against SARS-CoV-2 due to the urgency in disposing of a molecular arsenal to contrast the epidemic. In this sense, several molecules such as favipiravir [9], aprotinin [10], prolastin [11], losmapimod [12], hydroxychloroquine [13,14] are in clinical trial, while many other drugs, developed to different purposes, are being considered as potential anti-COVID-19 treatment based on in silico studies [15–17]. However, drug repositioning cannot represent the only strategy and it is evident how the identification and the development of new, specific anti-SARS-CoV-2 agents are nowadays mandatory [18].

SARS-CoV-2 genome is a positive-sense RNA strand codifying for 27 non-structural and structural proteins of which four play a pivotal role in infectious cycle and, therefore, considered as principal pharmacological targets. Specifically, the spike protein (SP) is an envelope glycoprotein involved in host receptor binding, the latter identified as angiotensin-converting enzyme 2 [15–17]. The blockage of spike function prevents the virus entry, spread, and effectiveness [19]. RNA-dependent RNA-polymerase (RdRp) is responsible for nucleic material replication and it is the only validated target for COVID-19 pharmacological treatment so far [20,21]. Finally, exploiting host machinery, SARS-CoV-2 RNA is translated into two large polyproteins (pp1a and pp1ab) that undergo a maturation process catalyzed by two different viral proteases: the 3 chymotrypsin-like protease ($3CL^{pro}$, also called main protease, M^{pro}) and the papain-like protease (PL^{pro}). The first is a cysteine protease responsible for catalytic Leu-Gly cleavages at the C-terminus of pps leading to 11 non-structural, mature proteins [22,23]. The second one, PL^{pro}, is involved in two non-structural proteins maturation by cleaving N-terminus sequences containing LeuXGlyGly↓(Ala/Leu)X motifs, where X is any type of amino acid [24,25]. The pivotal role of these enzymes together with the structural knowledge acquired about the inhibitor/protease complexes make them two of the most investigated druggable targets to contrast SARS-CoV-2.

Two classes of SARS-CoV-2 M^{pro} inhibitors have been developed so far: covalent and non-covalent inhibitors. The first comprises peptidomimetics designed to covalently interact with Cys145 in the catalytic site that share four features: a) moderate size; b) a group mimicking a glutamine side chain; c) a branched lipophilic group; d) a reactive electrophilic 'warhead', such as aldehydes, Michael acceptors, and epoxy ketones responsible for the covalent bond [25,26]. However, the possibility of non-specific biological interactions due to their huge reactivity, must be considered for the subsequent in vivo evaluation of this type of inhibitors [27,28]. Accordingly, the less reactive non-covalent inhibitors may represent safer antiviral agents. Indeed, despite the lack of covalent bond in the active site of protease, they can represent useful tools to counteract the virus as well [29–31].

Starting from these evidence, in the present paper we describe the design, synthesis and biological evaluation of a new series of indole-based derivatives designed as SARS-CoV-2 M^{pro} inhibitors. General structures of synthesized compounds are depicted in Fig. 1.

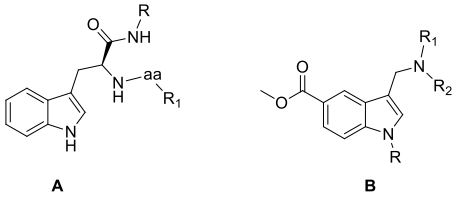

Fig. 1. General structures of synthesized compounds.

A series of peptidomimetics was synthesized starting from L-tryptophan that was functionalized with an amine moiety (R–NH_2) and a natural or modified amino acid (R1-aa, Fig. 1A). Two additional small molecules were synthesized starting from methyl 1H-indole-5-carboxylate that was derivatized in positions 1 and 3 to give the corresponding aminomethyl substituted derivatives (Fig. 1B). These compounds derived from a step-by-step in silico design coupled with the evaluation of enzymatic assay results. To further investigate their pharmacological properties, the compounds were tested in a Vero cells model to evaluate their ability to reduce the plaques formations and also gaining information about their cytotoxic behavior. This workflow led to the identification of two compounds as SARS-CoV-2 proteases inhibitors. First, compound **29** emerged as powerful, non-cytotoxic, SARS-CoV-2 multitarget inhibitor, showing high affinity both for M^{pro} and for PL^{pro}. Moreover, compound **34**, besides its interesting cellular activity, showed a high affinity and selectivity for SP.

2. Synthesis

Final compounds **7** and **22**–**29** were synthesized as summarized in Scheme 1. L-Boc-Trp-OH was coupled with *tert*-butyl amine, 4-phenylbenzylamine or benzylamine using HOBt and HBTU as coupling agents and DIPEA as base. Amides **1**–**3** were thus obtained in 65–80% yields. Removal of the Boc protecting group by DCM:TFA (3:1 v:v), gave intermediates **4**–**6** in almost quantitative yields. The intermediates were coupled, without further purification, with different L-aminoacids (L-Boc-Pro-OH, L-Boc-Phe-OH, L-Boc-Leu-OH, L-Boc-Pra-OH or L-Boc-allylgly-OH) using the same coupling protocol described above. In this way, final compound **7** (59% of yield) and pseudo peptides intermediates **8**–**14** (74–82% of yields) were obtained. Removal of the Boc protection from derivatives **8**–**14**, led to **15**–**21**, that were further derivatized by reductive amination with 4-phenyl benzaldehyde, benzaldehyde or propionaldehyde to give final derivatives **22**–**28** in 55–66% yields. Alternatively, acylation of **20** with chloroacetyl chloride led to compound **29** in 62% yield.

The synthetic route to obtain small molecules **34** and **35** is illustrated in Scheme 2. Using methyl 1H-indole-5-carboxylate as starting material, N-1 alkylation was performed by reaction with isobutyl iodide or methyl iodide using sodium hydride as base. In this way, intermediates **30** and **31** were synthesized in 80 and 82% yields, respectively. Starting from these compounds, Mannich reaction was carried out [32] leading to intermediates **32** and **33** in 70% and 75% yield, respectively. Upon alkylation with benzyl bromide, final compound **34** was obtained in 78% yield, while compound **35** resulted from a coupling reaction of **33** with L-propargyl glycine as described above and was isolated in 80% yield.

3. In silico design

With the aim of identifying novel antiviral agents against SARS-CoV-2, molecular docking experiments were performed against the related M^{pro} target (PDB code: 6M0K) [33]. Different studies

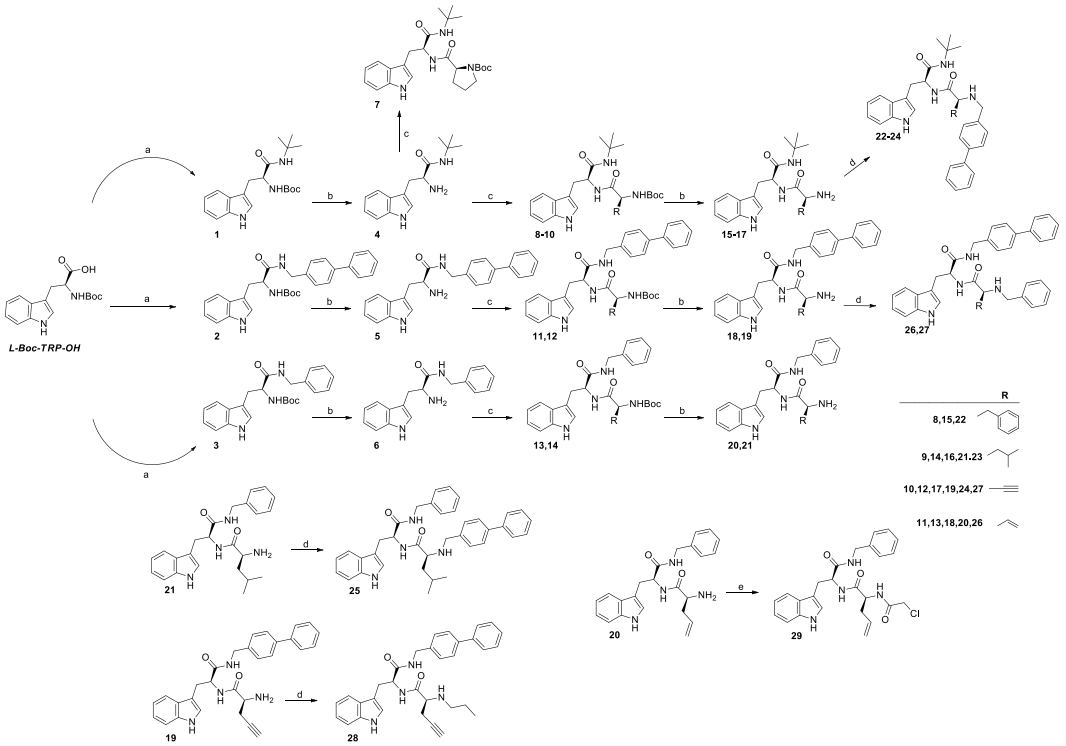

Scheme 1. Synthesis of final compounds **7, 22**–**29.** Reagents and conditions: a) HOBt (1.2 eq), HBTU (1.2 eq), DIPEA (2.4 eq), amine (1.2 eq), DCM, 12h, RT b) TFA/DCM (1/3, v/v), triisopropylsilane (0.25 eq), 30–120 min, RT c) HOBt (1.0 eq), HBTU (1.0 eq), DIPEA (2.0 eq), L-Boc-aa-OH (0.83 eq), DCM, 12h, RT d) RCOH (1.2 eq), MeOH, N_2 stream, RT, 12 h. Then, $NaBH_4$ (3.0 eq), RT, 3h e) TEA (1.2 eq), chloro acetylchloride (1.2 eq), THF, RT, 20 min.

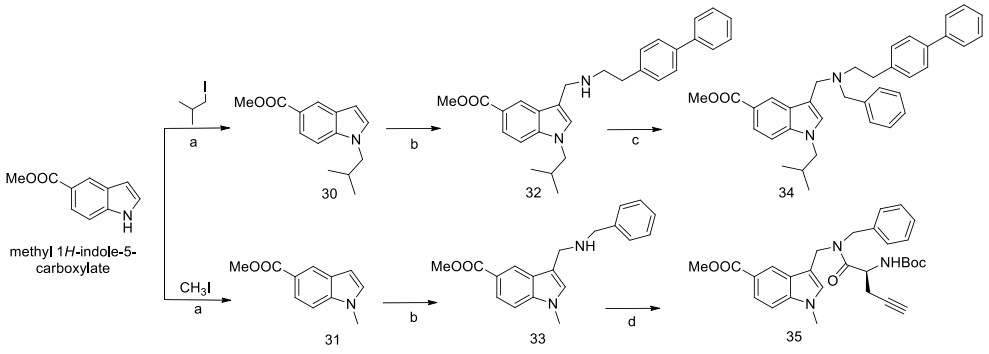

Scheme 2. Synthesis of final compounds **34** and **35.** Reagents and conditions: a) NaH (1.5 eq), alkyl iodide (1.5 eq), DMF, 0 °C to RT, overnight. b) Formaldehyde (2.0 eq), TFA (2.0 eq), amine (2.0 eq), DCM, 12h, RT. c) Aldehyde (1.2 eq), MeOH, N_2 stream, RT, 12 h. Then, $NaBH_4$ (3 eq), RT, 3h d) HOBt (1.2 eq), HBTU (1.2 eq), DIPEA (2.4 eq), L-Boc-Pra-OH (1.2 eq), DCM, 12h, RT.

focused on the discovery of new compounds able to interfere with this enzyme were recently reported, and the availability of different X-ray M^{pro}/inhibitor co-complex structures represented a precious source of information for orienting the design of novel compounds.

In 2020, Dai et al. reported the structure-based identification of two SARS-CoV-2 M^{pro} inhibitors (**A1** and **B1**, Fig. 2) [33], that covalently bound M^{pro} due to the presence of aldehyde moieties able to react with Cys145 key residue. Also, further specific chemical functions were introduced in precise positions in order to cover the whole binding site. It is worth noting that the analysis of the active sites of M^{pro}s revealed the high conservation among all coronavirus M^{pro}s, and they are usually composed of four sites: S1', S1, S2, and S4 (Fig. 2) [33,34]. The reactive Cys145 is placed in the S1' site, S1 and S2 sites can accommodate large and cyclic systems, while S4 site was prone to interact with specific moieties, such as indole substituent identified in this study [33]. Specifically, the latter was introduced to form hydrogen bonds with key residues in the S4 site and to improve drug-like properties.

Starting from these data, we performed molecular docking experiments to explore the binding mode of a series of new peptidomimetic compounds (Fig. 3 and Table S1). In details, the design and synthesis of the different derivatives were guided step-by-step by the outcomes obtained from enzymatic assays on the cognate compounds. Recursive cycles of in silico analysis, synthesis and biophysical analysis of target engagements were performed. Results are summarized in Table 1 and are compared with the IC_{50} of GC-376, a well-known M^{pro} inhibitor, used as reference compound.

In this way, the combination of in silico and experimental testing allowed the gradual generation of a small library of compounds sharing similar chemical functions and exhibiting

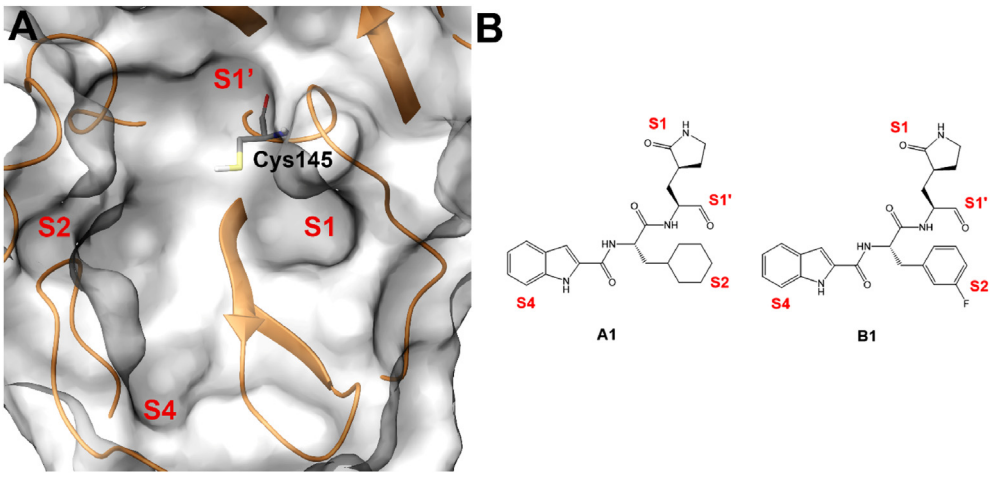

Fig. 2. A) SARS-CoV-2 M^{pro} binding site; S1', S1, S2, and S4 sites and Cys145 key residue are highlighted. B) Chemical structures of compounds **A1** and **B1**, with specified the chemical moieties interacting with the S1', S1, S2, and S4 M^{pro} sites.

promising activities against SARS-CoV-2 M^{pro}. Specifically, we firstly evaluated whether the L-tryptophan fragment could show a similar interaction network established by the reference compounds **A1** and **B1**, in particular regarding the placement of the indole function in the binding site. Unfortunately, molecular docking calculations highlighted that the indole moiety of capped L-Trp (**mtrp**) was placed in the S2 instead of S4 site (Fig. 3A). In order to force the 1H-indol-3-yl moiety in the S4 site, the L-Trp starting fragment was decorated introducing voluminous substituents at both the amino (N-) and carboxyl (C-) termini. After different attempts, satisfactory outcomes were obtained by linking the L-Leu at the L-Trp N-terminus and an N-benzyl moiety at the L-Trp C-function terminus. The introduction of a ([1,1′-biphenyl]-4-yl) substituent at the L-Leu N-terminus led to compound **25**, showing a good accommodation in the M^{pro} binding site (Fig. 3B). This compound was indeed able to cover S1', S1, S2, and S4 sites while also establishing a set of interactions with His41 and Cys145 (belonging to the catalytic dyad), Phe140, Glu166, and Gln189. The promising binding of compound **25** to M^{pro} was confirmed by enzymatic assays (Table 1), obtaining an IC_{50} value in the medium micromolar range of activity. Also, the careful analysis of the sampled binding poses of **25** disclosed that the terminal benzyl moiety could be replaced by a shorter and bulky substituent, finally leading to compound **23** (Fig. 3C) featuring a *tert*-butyl moiety. As expected, **23** showed a remarkable inhibitory activity against M^{pro} in the low micromolar range (1.73 μM, Table 1). The introduction of a bulkier and aromatic substituent (compound **22**, featuring the L-Phe residue instead of the L-Leu) determined a totally different predicted binding mode (Fig. 3D), thus indicating the poor ability of **22** in interfering with M^{pro} activity, as confirmed by enzymatic assays (Table 1). On the other hand, compound **7** showed an interaction network and a total shape of the molecule similar to that previously obtained for **23** (Fig. 3E). Such computational indications were confirmed by detecting the promising ability of **7** in interfering with the enzyme activity (Table 1).

Starting from the most promising compound **23** (Fig. 3C), we then wondered whether the introduction of a reactive chemical function able to covalently bind the Cys145 could lead to an improved biological activity. With this aim, the isobutyl moiety from L-Leu residue in **23** was replaced with a propyn-2-yl function (compound **24**), thus taking into account the reactivity of alkyne group with cysteine residues, as widely reported [35–37]. On the other hand, the analysis of the covalent complex revealed the loss of a series of key interactions with the key residues belonging to S1', S1, S2, and S4 sites as previously detected for **23** (Fig. 3F), and confirmed by poor outcomes from enzymatic assays (Table 1). Starting from compound **24**, we introduced the ([1,1′-biphenyl]-4-yl) substituent at the C-terminus while using a smaller benzyl moiety at the N-terminus (compound **27**). Covalent docking calculations showed a binding mode compatible with that previously observed for **23** (Fig. 3G), confirmed by the promising data from enzymatic experiments (Table 1). On the other hand, compound **26**, differing from **27** for the presence of an alkene function instead of the alkyne one, usually showing a reversible covalent behavior [38], showed a poor interference with the protein counterpart, as expected. Specifically, while covalent docking calculations revealed an interaction pattern similar to that established by **27**, the poses related to the non-covalent complex highlighted the loss of most of the interactions with the protein counterpart (e.g., His41) (Fig. 3H) and, for these reasons, we speculated that the observed poorer activity could be ascribed to this latter binding mode. The replacement of the benzyl substituent in **27** with an alkyl function (compound **28**) determined the loss of a series of key interactions with the protein counterpart (Fig. 3I), again leading to a reduced inhibitory activity. Instead, the introduction of a further putative covalent attachment point (α-chloroketone moiety, compound **29**) led to a promising binding related to the irreversible complex (Fig. 3J), subsequently corroborated by enzymatic assay data (Table 1).

Eventually, two small molecules (compounds **34** and **35**), obtained according to the synthetic route reported in the chemistry section (Table 1), were evaluated. Specifically, the indole function was modified introducing alkyl substituents on the basic nitrogen while also showing an ester function at C-5 position. As expected, molecular docking calculations highlighted that such modifications led to a poor predicted binding with the protein counterpart, especially for what concerned the interaction network in the S4 site, since the modified indole moiety pointed in a region between the S2 and S1' site (Fig. 3K). For what concerns compound **35**, the poses arising from covalent docking calculations again highlighted the contacts between the modified indole moiety with the residues close to the S1 site, thus again not in accordance with the interaction network detected for the most promising compounds (e.g., **7**, **23**, **27**, **29**) (Fig. 3L). As expected, for both the compounds, biological experiments highlighted the absence of inhibitory activity (Table 1).

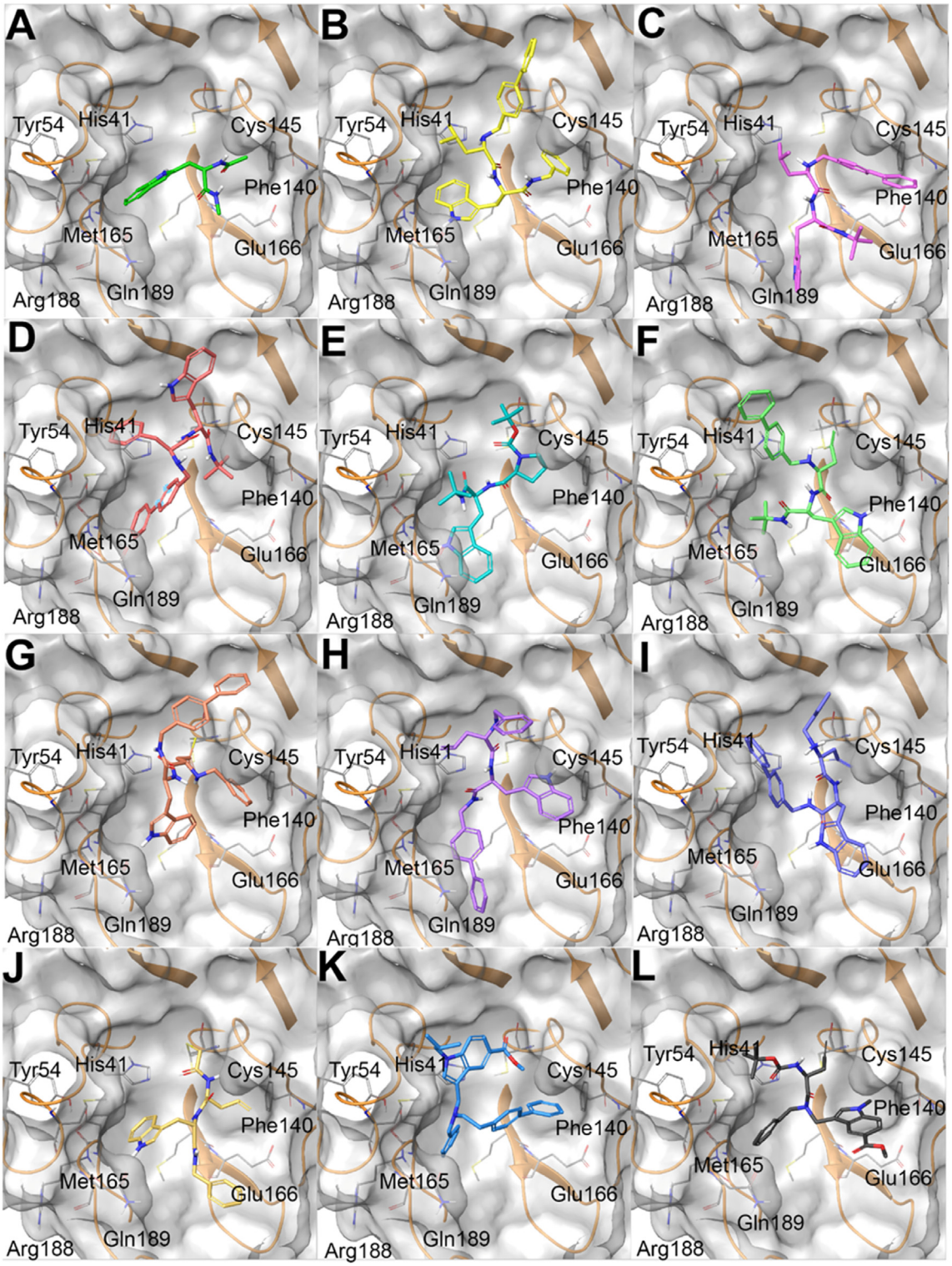

Fig. 3. A) **mtrp** (colored by atom type: C green, O red, N blue, polar H light grey), B) **25** (colored by atom type: C yellow, O red, N blue, polar H light grey); C) **23** (colored by atom type: C purple, O red, N blue, polar H light grey); D) **22** (colored by atom type: C pink, O red, N blue, polar H light grey); E) **7** (colored by atom type: C aqua green, O red, N blue, polar H light grey); F) **24** (colored by atom type: C light green, O red, N blue, polar H light grey); G) **27** (colored by atom type: C light brown, O red, N blue, polar H light grey); H) **26** (colored by atom type: C light violet, O red, N blue, polar H light grey); I) **28** (colored by atom type: C violet, O red, N blue, polar H light grey); J) **29** (colored by atom type: C light yellow, O red, N blue, polar H light grey); K) **34** (colored by atom type: C light blue, O red, N blue, polar H light grey); L) **35** (colored by atom type: C dark grey, O red, N blue, polar H light grey) in docking with SARS-CoV-2 M^{pro} (transparent molecular surface colored in grey and secondary structure colored in orange; key residues are reported as sticks and colored by atom type: C grey, O red, N blue, S yellow, polar H light grey).

Table 1
Measured activities for inhibition of SARS-CoV-2 selected protein targets. Results are reported as average ± SD.

Compound	Structure	Target protein		
		M^{pro}	PL^{pro}	SP
		IC_{50} (μM)	IC_{50} (μM)	K_D (μM)
GC-376		**0.57 ± 0.15**	–	–
GRL-0617		–	**1.67 ± 0.63**	–
7	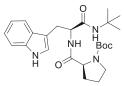	**5.01 ± 2.31**	>25	>25
22	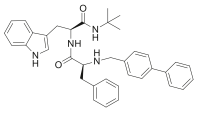	>25	>25	19.05 ± 0.41
23	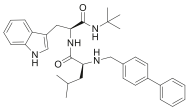	**1.73 ± 0.89**	>25	>25
24	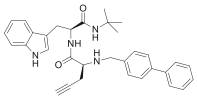	>25	>25	>25
25	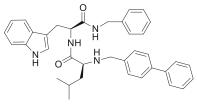	23.61 ± 8.72	>25	–
26	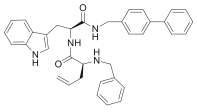	>25	>25	>25
27	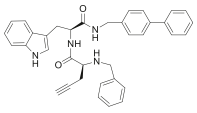	**2.86 ± 1.42**	>25	–
28	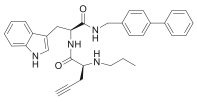	22.65 ± 9.82	>25	–
29	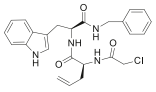	**1.72 ± 0.75**	**0.67 ± 0.59**	**> 25**
34	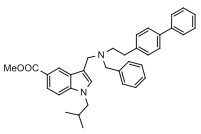	>25	>25	**3.26 ± 0.11**
35	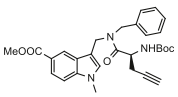	>25	>25	**11.41 ± 0.36**

4. Pharmacological characterization in SARS-CoV-2 transfected cells

To further expand the results obtained in-vitro, the synthesized compounds were challenged in a more relevant biological environment. A cellular screening using Vero cells transfected with two different clinical isolates of SARS-CoV-2 (UC-1074 and UC-1075 strains) was performed. The EC_{50} of the synthesized compounds was calculated along with the determination of cell morphology and cell growth. Remdesivir was used as positive control. Results obtained are summarized in Table 2.

Despite the remarkable activity showed in enzymatic assays, compounds **7** and **23** largely failed to inhibit viral plaque formation with compound **23** showing high cytotoxicity. These data could be probably justified on the basis of the predominant lipophilic character of the two compounds, determining unfavorable pharmacokinetic properties as well as precipitation and/or aggregation in the cellular medium [39,40]. On the other hand, compounds **27** and **29**

Table 2
Cellular assays results.

Compound	Antiviral activity EC_{50}[a] UC-1074 #1 strain Vero cells	Antiviral activity EC_{50}[a] UC-1075 #1 strain Vero cells	Cytotoxicity	
	15 μl/10 mL	100 μl/10 mL	Cell morphology (MCC)[b]	Cell growth (CC_{50})[c]
Remdesivir	0.87 μM	0.61 μM	>40 μM	>40 μM
7	>100 μM	>100 μM	>100 μM	>100 μM
22	**2.19 μM**	**2.01 μM**	**> 100 μM**	**1.49 μM**
23	>4 μM	>4 μM	20 μM	10.61 μM
24	>4 μM	>4 μM	20 μM	4.67 μM
25	>4 μM	>20 μM	≥20 μM	34.70 μM
26	63.14 μM	>20 μM	≥100 μM	78.37 μM
27	**8.94 μM**	**10.94 μM**	**≥ 100 μM**	**51.52 μM**
28	>20 μM	>20 μM	>100 μM	42.35 μM
29	**0.32 μM**	**1.37 μM**	**100 μM**	**38.67 μM**
34	**5.98 μM**	**0.44 μM**	**100 μM**	**31.53 μM**
35	4 μM	20 μM	100 μM	8.09 μM

[a] Effective concentration required to reduce virus plaque formation by 50%. Virus input was 100 $CCID_{50}$.
[b] Minimum cytotoxic concentration that causes a microscopically detectable alteration of cell morphology.
[c] Cytotoxic concentration required to reduce cell growth by 50%.

confirmed the antiviral activity showed in-vitro. In particular, compound **29** potency was comparable to remdesivir and 28-fold higher than compound **27** over two different SARS-CoV-2 strains, with negligible cytotoxicity. Moreover, derivatives **22** and **34**, that were unable to antagonize M^{pro} in-vitro, showed cellular antiviral activity. Besides results for derivative **22** were largely affected by high cytotoxicity (Table 2), compound **34** antiviral activity was worth of further investigations.

Thus, we questioned whether the synthesized compounds were also able to bind different SARS-CoV-2 target proteins, namely PL^{pro} and SP. As reported in Table 1, compound **29** showed remarkable affinity for the PL^{pro} with lower EC_{50} than the reference compound GRL-0617. This dual inhibitory effect is likely responsible for the higher cellular antiviral activity of **29**, when compared to **23**, highlighting the potential of dual M^{pro} and PL^{pro} inhibitors as anti SARS-CoV-2 therapeutics.

In order to rationalize these data, molecular docking calculations were performed for compound **29** against SARS-CoV-2 PL^{pro}. Specifically, two different models, related to the non-covalent and covalent binding, were generated. In the non-covalent ligand/protein complex (PDB code: 7JIW) [41], compound **29** was accommodated in the binding site of the protein establishing a large set of interactions, namely π-π stacking with Tyr268, π-cation with Arg166, H-bonds with Gln269 and Thr301 (Fig. 4A). Furthermore, the comparison of the binding modes of the tested compound and of the compound VBY originally co-crystallized in the protein structure highlighted similar ligand shapes [41], thus confirming the promising interaction of **29** with SARS-CoV-2 PL^{pro}. On the other hand, to shed light on the hypothetical covalent binding, the SARS-CoV-2 PL^{pro} covalently co-complexed with a peptide inhibitor (PDB code: 6WX4) through the reactive Cys111 residue was accounted [24]. In this case, the output poses arising from covalent docking calculations highlighted a different binding mode and, in particular, the indole and benzyl functions were oriented towards the external part of the protein, while also establishing H-bonds with Gly271 and His272 (belonging to the catalytic triad of this enzyme), and π-π stacking with Trp106 (Fig. 4B, Table S2).

Interestingly, we found that the cellular inhibitory effects of compound **34**, is due to its ability to selectively inhibit SARS-CoV-2 spike protein in the low micromolar range (Table 1). The small molecule **34** could be thus considered an interesting chemotype for the development of a new class of anti-SARS-CoV-2 agents, selectively inhibiting SP.

Molecular docking calculations were performed accounting the SP receptor-binding domain structure released by Wang et al. (PDB code: 6LZG) originally co-complexed with ACE2 [42]. In silico

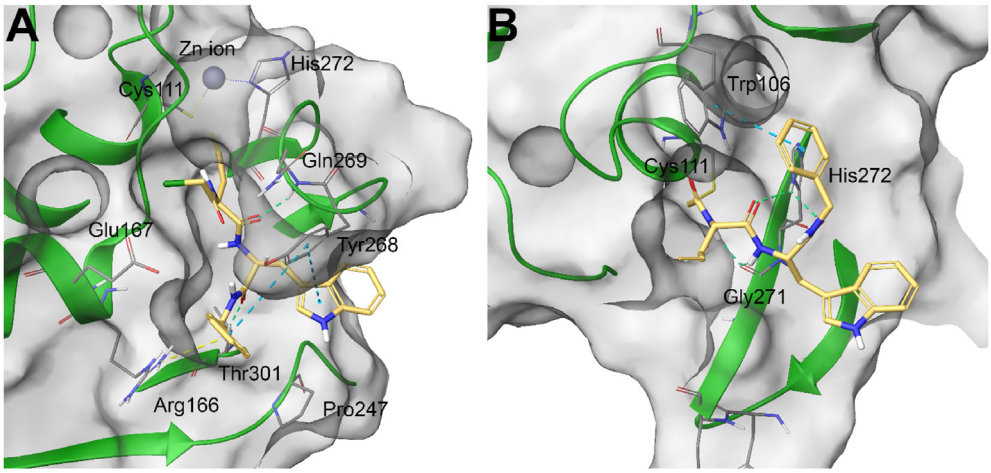

Fig. 4. A) non-covalent and B) covalent molecular docking complexes between **29** (colored by atom type: C light yellow, O red, N blue, polar H light grey) and SARS-CoV-2 PL^{pro} (transparent molecular surface colored in grey and secondary structure colored in green; key residues are reported as sticks and colored by atom type: C grey, O red, N blue, S yellow, polar H light grey).\

experiments highlighted the accommodation of **34** featuring a good shape complementarity with the external surface of SP and a large network of contacts with some residues responsible of the SP-ACE2 protein-protein interaction (Fig. 5). Specifically, **34** made π-π stacking with Phe459 and Tyr348 and H-bond with Glu484 as well as a large set of hydrophobic and polar contacts with Tyr449, Leu455, Phe486, Gln493, and Ser494 (Fig. 5, Table S3).

Finally, compounds **27**, **29** and **34** were also tested for their antiviral activity over Vero cells infected with CMV and VZV strains, to assess their selectivity. The compounds proved to be selective SARS-CoV-2 antiviral agents with no effects over cytomegalovirus and varicella zoster virus (data not shown).

5. Discussion

Different druggable targets of SARS-CoV-2 have been identified so far and several modulators have been described [15,16,43–45]. First attempts were focused on SARS-CoV-2 spike protein, RdRp (RNA dependent RNA polymerase), and M^{pro} targeting [46]. Despite little evidence has been collected about the clinical efficacy of these molecules, researchers largely agree about their limitations due to the rapid viral mutations, underlying resistance. In this context, the development of multitarget inhibitors, able to target different proteins belonging to the viral machinery has been explored as a suitable strategy to overcome viral resistance, improve the overall anti-viral efficacy and largely reduce the multi-drug dose burden [47–50]. Moreover, less focus has been given, initially, to other important proteases, such as PL^{pro}, that equally play a pivotal role in the viral replication processes [46,48]. M^{pro} and PL^{pro} represent two cysteine proteases of the virus, that process the C-terminal of replicase apo-polyprotein to yield the active functional proteins necessary for viral replication and, hence, for infection spreading. Thus, simultaneous inhibition of these proteases may significantly hamper the viral machinery and represents a valuable therapeutic option to SARS-CoV-2 tackling. Some of such dual inhibitors, obtained by drug repurposing or de-novo synthesis, have been yet described. In particular, a library of ebselen derivatives has been synthesized to specifically identify dual M^{pro} and PL^{pro} inhibitors [51]. These molecules showed nanomolar potency over M^{pro}, while were thousand-fold less potent over PL^{pro}. Cellular screenings have not been performed for these molecules and there is a general lack of knowledge concerning their efficacy and safety in a relevant biological environment, though ebselen is largely considered non-cytotoxic. On the other hand, drug repurposing in silico protocols have highlighted some natural and synthetic products as dual M^{pro} and PL^{pro} inhibitors [52,53]. Ginkgolic and anacardic acids, in particular, showed moderate potencies in enzymatic assays, especially over PL^{pro}, cellular plaque formation IC_{50}s in the high micromolar range, but also comparable CC_{50} values [52]. Ma and coworkers also showed that several compounds identified through in silico screening as potential multitarget proteases inhibitors completely lack of cellular antiviral activity, despite the high potencies showed in enzymatic assays. This is probably due to nonspecific oxidation or alkylation of the cysteine residue in the protease catalytic pocket by reactive compounds [53]. In this context compound **29** represents an advancement of the existing knowledge, being a synthetic molecule with a comparable in-vitro inhibitory potency against M^{pro} and PL^{pro} and a remarkable ability in reducing viral plaques formation in Vero cells. These antiviral properties are further strengthened by reduced cytotoxicity and good selectivity over other viruses, making derivative **29** an interesting hit compound for the development of anti-SARS-CoV-2 therapeutics. In silico studies, indeed, provided important SAR clues for the rational development of a new class of specific dual proteases inhibitors. On the other side, the extended investigations carried on the synthesized compounds, also led to the identification of compound **34** as a promising selective SARS-CoV-2 spike protein inhibitor, deserving further development in consideration of the binding mode described and the specific drug/target interactions evidenced.

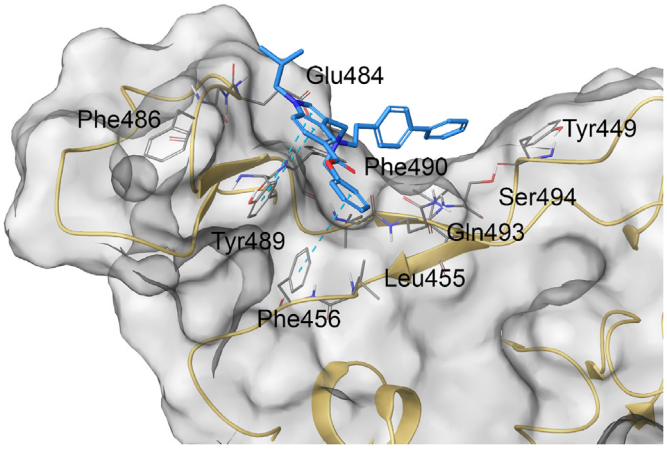

Fig. 5. Molecular docking complex between **34** (colored by atom type: C light blue, O red, N blue, polar H light grey) and SARS-CoV-2 SP (transparent molecular surface colored in grey and secondary structure colored in light yellow; key residues are reported as sticks and colored by atom type: C grey, O red, N blue, S yellow, polar H light grey).

6. Experimental section

6.1. General

All reagents and solvents used were purchased from Sigma-Aldrich (Milan, Italy). Reactions were performed under magnetic stirring in round-bottomed flasks unless otherwise noted. Moisture sensitive reactions were conducted in oven-dried glassware under nitrogen stream, using distilled solvents. Purifications were conducted on the Biotage Isolera One flash purification system, using prepacked KP-sil columns, (Biotage, Uppsala, Sweden). TLC analysis were performed on precoated glass silica gel plates 60 (F254, 0.25 mm, VWR International). 1D-NMR spectra were recorded with Bruker Avance (400 MHz) spectrometer, at room temperature. Chemical shifts were reported in δ values (ppm) relative to internal Me_4Si for 1H and 13C NMR. J values were reported in hertz (Hz). The following abbreviations are used to describe peaks: s (singlet), d (doublet), dd (doublet of doublets), t (triplet), q (quartet), and m (multiplet). HR-MS experiments were performed using an LTQ-Orbitrap-XL-ETD mass spectrometer (Thermo Scientific, Bremen, Germany), using electrospray ionization. Elemental analysis was carried on using a PerkinElmer 2400 Series II CHNS/O analyzer. Results obtained were within ±0.4% of theoretical values.

6.1.1. General procedure A: coupling reactions

1 mmol of various N-L-Boc amino acids was dissolved in dichloromethane and HOBt (1.2 eq), HBTU (1.2 eq), DIPEA (2.4 eq) and the corresponding amine (1.2 eq) were added and stirred at room temperature for 12 h. Then, the solvent was evaporated in vacuum, and the residue was dissolved in dichloromethane and washed with water (3 × 200 mL), a saturated solution of $NaHCO_3$ (3 × 200 mL), and a solution of citric acid (10% w:w, 3 × 200 mL). The organic phase was extracted, dried over Na_2SO_4, filtered, and concentrated under vacuum. The crude products were purified by flash chromatography using mixtures of n-hexane/ethyl acetate as mobile phase [54].

6.1.2. General procedure B: Boc removal

The N-Boc protected intermediate (0.2 mmol) was dissolved in a mixture of TFA/DCM (1/3, v/v), and added with triisopropylsilane (0.25 equiv). Reaction was stirred at room temperature for 2h. Then, a solution of NaOH (2 N) was added until pH 7. The mixture was diluted with water and dichloromethane, and the organic phase was extracted, dried over Na_2SO_4, filtered, and concentrated under vacuum. The intermediates obtained were not further purified.

6.1.3. General procedure C: reductive amination

The proper intermediate (1 mmol) was dissolved in MeOH dry and 1.2 equivalents of the proper aldehyde were added. The mixture was allowed to react for 12h under nitrogen stream, at room temperature. Then, 3 equivalents of $NaBH_4$ were added portionwise and the mixture was stirred for further 3h. The reaction was quenched by 10% aqueous solution of citric acid, the solvent was evaporated in vacuum, and the residue was dissolved in dichloromethane and washed with water (3 × 200 mL). Organic layer was separated, dried over anhydrous Na_2SO_4, filtered, and evaporated in vacuo. The crude products were purified by column chromatography using mixtures of ethyl acetate/n-hexane as eluent.

6.1.4. General procedure D: N-alkylation

Methyl indole-5-carboxylate (1.0 mmol) was dissolved in anhydrous DMF under magnetic stirring at 0 °C. To this solution, 1.5 equivalents of NaH and 1.5 equivalents of iodomethane or 1-iodo-2-methylpropane in DMF were added dropwise and the reaction was warmed to room temperature and maintained under stirring overnight. The reaction was quenched by 10% aqueous solution of citric acid and washed with brine. Organic layer was separated, dried over anhydrous Na_2SO_4, filtered, and evaporated in vacuo. Crude products were purified by column chromatography.

6.1.5. General procedure E: Mannich reactions

A solution of formaldehyde (2.0 eq), trifluoroacetic acid (2.0 eq) and amine (2.0 eq) in dichloromethane was stirred at room temperature for 30 min. Then, a solution of the proper 1,5-disubstituted indole (1 mmol) in dichloromethane was added and the mixture was stirred for 12h. The reaction was quenched by 10% aqueous solution of sodium bicarbonate and washed with brine, dried over anhydrous Na_2SO_4 and filtered. Organic phase was evaporated in vacuum and 3-aminomethyl indole derivatives were obtained after purification by flash chromatography.

6.1.5.1. tert-butyl (1-(tert-butylamino)-3-(1H-indol-3-yl)-1-oxopropan-2-yl)carbamate (1). Synthesized according to the general procedure **A**, using Boc-L-Trp-OH and *tert*-butylamine as starting materials, FC in n-hexane/ethyl acetate 3/1, Rf = 0.35. Yellowish oil (65% yield). ^{1}H NMR (400 MHz, $CDCl_3$): δ: 1.14 (s, 9H, CH_3); 1.46 (s, 9H, CH_3); 3.07–3.12 (m, 1H, CH_{2a}); 3.30–3.35 (m, 1H, CH_{2b}); 4.36 (bs, 1H, CH); 5.37 (bs, 1H, NH); 7.06 (s, 1H aryl); 7.15 (t, 1H, aryl, J = 7.2 Hz); 7.22 (t, 1H, aryl, J = 7.4 Hz); 7.39 (d, 1H, aryl, J = 8.2 Hz); 7.72 (d, 1H, aryl, J = 6.8 Hz); 8.43 (bs, 1H, NH). HR-MS m/z calcd for $C_{20}H_{30}N_3O_3$ [(M + H)]$^+$: 360.2282; found 360.2277.

6.1.5.2. (S)-tert-butyl (1-(([1,1′-biphenyl]-4-ylmethyl)amino)-3-(1H-indol-3-yl)-1-oxopropan-2-yl)carbamate (2). Intermediate **2** was obtained according to the general procedure **A**, starting from Boc-L-Trp-OH and 4-phenyl benzylamine, FC in n-hexane/ethyl acetate 3/1, Rf = 0.4. Yellowish oil (82% yield). ^{1}H NMR (400 MHz, $CDCl_3$): δ: 1.44 (s, 9H, CH_3); 3.22 (dd, 1H, CH_{2a}, J' = 7.7, J'' = 14.4 Hz); 3.38 (dd, 1H, CH_{2b}, J' = 5.3, J'' = 14.4 Hz); 4.30–4.36 (m, 2H, CH_2); 4.49 (bs, 1H, CH); 5.20 (bs, 1H, NH); 6.05 (bs, 1H, NH); 7.02 (s, 1H aryl); 7.17 (d, 1H, aryl, J = 7.6 Hz); 7.19 (t, 1H, aryl, J = 7.8 Hz); 7.24 (t, 1H, aryl, J = 7.8 Hz); 7.35–7.40 (m, 2H, aryl); 7.44–7.48 (m, 5H, aryl); 7.56 (d, 2H, aryl, J = 8.5 Hz); 7.71 (d, 1H, aryl, J = 7.8 Hz); 8.07 (bs, 1H, NH). HR-MS m/z calcd for $C_{29}H_{32}N_3O_3$ [(M + H)]$^+$: 470.2438; found 470.2445.

6.1.5.3. (S)-tert-butyl (1-(benzylamino)-3-(1H-indol-3-yl)-1-oxopropan-2-yl)carbamate (3). Synthesized according to the general procedure A, starting from Boc-L-Trp-OH and benzylamine.

FC in n-hexane/ethyl acetate 3/1, Rf = 0.4. Yellowish oil (80% yield). ^{1}H NMR (400 MHz, CD_3OD): δ: 1.40 (s, 9H, CH_3); 3.10 (dd, 1H, CH_{2a}, J' = 6.6, J'' = 13.8 Hz); 3.25 (dd, 1H, CH_{2b}, J' = 6.9, J'' = 14.4 Hz); 4.19–4.23 (m, 1H, CH); 4.34–4.41 (m, 2H, CH_2); 7.02–7.06 (m,5H, aryl); 7.12 (t, 1H, aryl, J = 7.1 Hz); 7.20–7.25 (m, 2H, aryl); 7.37 (d, 1H, aryl, J = 8.1 Hz); 7.62 (d, 1H, aryl, J = 7.8 Hz). HR-MS m/z calcd for $C_{23}H_{28}N_3O_3$ [(M + H)]$^+$: 394.2125; found 394.2114.

6.1.5.4. tert-butyl (1-(tert-butylamino)-3-(1H-indol-3-yl)-1-oxopropan-2-yl)carbamate (4). Intermediate **4** was synthesized according to the general procedure **B**, starting from **1**. White powder (90% yield). ^{1}H NMR (400 MHz, $CDCl_3$): δ: 1.22 (s, 9H, CH_3); 3.10 (dd, 1H, CH_{2a} J' = 7.8, J'' = 14.5 Hz); 3.30 (dd, 1H, CH_{2b} J' = 5.9, J'' = 14.5 Hz); 3.86 (t, 1H, CH, J = 6.7 Hz); 5.09 (bs, 2H, NH_2); 6.78 (s, 1H aryl); 7.10–7.17 (m, 2H, aryl); 7.36 (d, 1H, aryl, J = 8.1 Hz); 7.64 (d, 1H, aryl, J = 7.8 Hz); 8.92 (bs, 1H, NH). HR-MS m/z calcd for $C_{15}H_{22}N_3O$ [(M + H)]$^+$: 260.1757; found 260.1750.

6.1.5.5. (S)–N-([1,1′-biphenyl]-4-ylmethyl)-2-amino-3-(1H-indol-3-yl)propanamide (5). Intermediate **5** was synthesized according to the general procedure **B**, starting from **2**. White powder (91% yield). ^{1}H NMR (400 MHz, CD_3OD): δ: 3.27–3.35 (m, 1H, CH_{2a}); 3.42 (dd, 1H, CH_{2b}, J' = 7.6, J'' = 14.4 Hz); 4.16 (t, 1H, CH, J = 7.4 Hz); 4.31 (d, 1H, CH_{2a}, J = 14.8 Hz); 4.40 (d, 1H, CH_{2b}, J = 14.8 Hz); 7.07–7.19 (m, 6H aryl); 7.41–7.45 (m, 3H, aryl); 7.50 (d, 2H, aryl, J = 8.2 Hz); 7.58 (d, 2H, aryl, J = 7.2 Hz); 7.66 (d, 1H, aryl, J = 7.9 Hz). HR-MS m/z calcd for $C_{24}H_{24}N_3O$ [(M + H)]$^+$: 370.1914; found 370.1907.

6.1.5.6. (S)-2-Amino-N-benzyl-3-(1H-indol-3-yl)propanamide (6). Intermediate **6** was synthesized according to the general procedure **B**, starting from **3**. White powder (95% yield). 1H NMR (400 MHz, CD_3OD): δ: 3.05 (dd, 1H, CH_{2a}, J' = 5.8, J'' = 10.4 Hz); 3.20 (dd, 1H, CH_{2b}, J' = 6.0, J'' = 10.4 Hz); 3.69 (t, 1H, CH, J = 5.2 Hz); 4.25 (d, 1H, CH_{2a}, J = 12.6 Hz); 4.35 (d, 1H, C$H_{2b,}$ J = 12.6 Hz); 7.02–7.07 (m, 5H, aryl); 7.12 (t, 1H, aryl, J = 7.2 Hz); 7.20–7.26 (m, 2H, aryl); 7.39 (d, 1H, aryl, J = 8.2 Hz); 7.64 (d, 1H, aryl, J = 8.0 Hz). HR-MS m/z calcd for $C_{18}H_20N_3O$ [(M + H)]$^+$: 294.1601; found 294.1610.

6.1.5.7. tert-butyl 2-((1-(tert-butylamino)-3-(1H-indol-3-yl)-1-oxopropan-2-yl)carbamoyl)pyrrolidine-1-carboxylate (7). Final product **7** was synthesized starting from **1** and L-Boc-Pro-OH, following the procedure **A**. FC dichloromethane/methanol 4.8/0.2, Rf = 0.40. Yellow oil (59% yield). (**A**) ^{1}H NMR (400 MHz, CD_3OD): δ: 1.27 (s, 9H, CH_3); 1.29 (s, 9H, CH_3); 1.64–1.89 (m, 2H, CH_2); 2.11–2.20 (m, 2H, CH_2); 3.03–3.39 (m, 4H, CH_2); 4.08–4.10 (m, 1H, CH); 4.54–4.57 (m, 1H, CH); 7.05–7.17 (m, 3H, aryl); 7.33–7.40 (m, 1H, aryl); 7.60–7.69 (m, 1H, aryl). (**B**) ^{1}H NMR (400 MHz, CD_3OD): δ: 1.21 (s, 9H, CH_3); 1.34 (s, 9H, CH_3); 1.64–1.89 (m, 4H, CH_2); 3.03–3.39 (m, 4H, CH_2); 4.14–4.16 (m, 1H, CH); 4.63–4.65 (m, 1H, CH); 7.05–7.17 (m, 3H, aryl); 7.33–7.40 (m, 1H, aryl); 7.60–7.69 (m, 1H, aryl).^{13}C NMR (100 MHz, CD_3OD) δ 22.3, 23.0, 23.9, 26.2, 27.1, 27.4, 28.0, 29.5, 29.7, 30.9, 54.4, 60.4, 60.7, 80.1, 108.4, 109.4, 110.8, 111.2, 117.7, 118.1, 118.4, 118.8, 121.1, 121.3, 123.3, 123.5, 124.7, 127.6, 136.6, 154.6, 155.2, 171.3, 173.2, 173.8. HR-MS m/z calcd for $C_{25}H_{37}N_4O_4$ [(M + H)]$^+$: 457.2809; found 457.2801.

6.1.5.8. tert-butyl (1-((1-(tert-butylamino)-3-(1H-indol-3-yl)-1-oxopropan-2-yl)amino)-1-oxo-3-phenylpropan-2-yl)carbamate (8). Obtained from **4** and L-Boc-Phe-OH following the general procedure **A**. FC in n-hexane/ethyl acetate 3/1, Rf = 0.44. Yellowish oil (78% yield). ^{1}H NMR (400 MHz, DMSO): *δ*: 1.18 (s, 9H, C*H*$_3$); 1.29 (s, 9H, C*H*$_3$); 2.67–2.73 (m, 1H, C*H*$_{2a}$); 2.89 (dd, 1H, C*H*$_{2b}$ *J'* = 4.2, *J"* = 13.8 Hz); 2.95–3.07 (m, 2H, C*H*$_2$); 4.08–4.13 (m, 1H, C*H*); 4.48–4.53 (m, 1H, C*H*); 6.92–6.99 (m, 2H aryl); 7.06 (t, 1H, aryl, *J* = 7.9 Hz); 7.14–7.26 (m, 3H, aryl); 7.31 (d, 1H, aryl, *J* = 8.0 Hz); 7.43 (s, 1H, aryl); 7.58 (d, 1H, aryl, *J* = 8.0 Hz); 7.80 (d, 1H, aryl, *J* = 7.8 Hz); 10.81 (bs, 1H, N*H*). HR-MS *m/z* calcd for $C_{29}H_{39}N_4O_4$ $[(M + H)]^+$: 507.2966; found 507.2974.

6.1.5.9. tert-butyl (1-((1-(tert-butylamino)-3-(1H-indol-3-yl)-1-oxopropan-2-yl)amino)-4-methyl-1-oxopentan-2-yl)carbamate (9). Obtained from **4** and L-Boc-Leu-OH following the general procedure **A**. FC in n-hexane/ethyl acetate 2/1, Rf = 0.35. Yellowish oil (74% yield). ^{1}H NMR (400 MHz, $CDCl_3$): *δ*: 0.92–0.95 (m, 6H, C*H*$_3$); 1.17 (s, 9H, C*H*$_3$); 1.35 (s, 9H, C*H*$_3$); 1.64–1.67 (m, 1H, C*H*); 1.79–1.87 (m, 2H, C*H*$_2$); 3.08 (dd, 1H, C*H*$_{2a}$ *J'* = 8.0, *J"* = 14.4 Hz); 3.39–3.44 (m, 1H, C*H*$_{2b}$); 4.03–4.07 (m, 1H, C*H*); 4.63 (q, 1H, C*H*, *J* = 7.9 Hz); 4.71 (d, 1H, N*H*, *J* = 6.9 Hz); 5.62 (bs, 1H, N*H*); 7.09 (s, 1H, aryl); 7.17 (t, 1H, aryl, *J* = 7.6 Hz); 7.23 (d, 1H, aryl, *J* = 7.4 Hz); 7.39 (d, 1H, aryl, *J* = 8.0 Hz); 7.73 (d, 1H, aryl, *J* = 7.6 Hz); 8.22 (bs, 1H, N*H*). HR-MS *m/z* calcd for $C_{26}H_{41}N_4O_4$ $[(M + H)]^+$: 473.3122; found 473.3109.

6.1.5.10. tert-butyl ((S)-1-(((S)-1-(tert-butylamino)-3-(1H-indol-3-yl)-1-oxopropan-2-yl)amino)-1-oxopent-4-yn-2-yl)carbamate (10). Compound **10** was obtained using general procedure **A**, starting from intermediate **4** which was reacted with N-Boc-L-propargylglycine. FC in n-hexane/ethyl acetate 2/1, Rf = 0.36. Yellowish oil (80% yield). ^{1}H NMR (400 MHz, $CDCl_3$): *δ*: 1.18 (s, 9H, C*H*$_3$); 1.36 (s, 9H, C*H*$_3$); 2.08 (s, 1H, C*H*); 2.56–2.62 (m, 1H, C*H*$_{2a}$); 2.81–2.85 (m, 1H, C*H*$_{2b}$); 3.08 (dd, 1H, C*H*$_{2a}$ *J'* = 7.8, *J"* = 14.4 Hz); 3.46–3.51 (m, 1H, C*H*$_{2b}$); 4.22–4.24 (m, 1H, C*H*); 4.63–4.69 (m, 1H, C*H*); 5.24 (d, 1H, N*H*, *J* = 4.8 Hz); 5.62 (bs, 1H, N*H*); 7.09 (s, 1H, aryl); 7.16 (t, 1H, aryl, *J* = 7.9 Hz); 7.23 (t, 1H, aryl, *J* = 7.8 Hz); 7.39 (d, 1H, aryl, *J* = 8.0 Hz); 7.75 (d, 1H, aryl, *J* = 7.7 Hz); 8.43 (bs, 1H, N*H*). HR-MS *m/z* calcd for $C_{25}H_{35}N_4O_4$ $[(M + H)]^+$: 455.2653; found 455.2660.

6.1.5.11. tert-butyl ((S)-1-(((S)-1-(([1,1'-biphenyl]-4-ylmethyl) amino)-3-(1H-indol-3-yl)-1-oxopropan-2-yl)amino)-1-oxopent-4-en-2-yl)carbamate (11). Obtained from **5** and Boc-L-allylgly-OH following the general procedure **A**. FC in hexane/ethyl acetate 3/1, Rf = 0.45. White powder (75% yield). ^{1}H NMR (400 MHz, CD_3OD): *δ*: 1.36 (s, 9H, C*H*$_3$); 2.21–2.26 (m, 1H, C*H*$_{2a}$); 2.28–2.36 (m, 1H, C*H*$_{2b}$); 3.02 (dd, 1H, C*H*$_{2a}$, *J'* = 7.4, *J"* = 14.4 Hz); 3.14 (dd, 1H, C*H*$_{2b}$, *J'* = 6.5, *J"* = 14.4 Hz); 3.96–4.02 (m, 1H, C*H*); 4.21–4.32 (m, 2H, C*H*$_2$); 4.62 (q, 1H, C*H*, *J* = 7.2 Hz); 4.96–5.04 (m, 2H, C*H*$_2$); 5.61–5.73 (m, 1H, C*H*); 6.87 (d, 1H, aryl, *J* = 8.1 Hz); 6.99 (t, 1H, aryl, *J* = 7.5 Hz); 7.07 (t, 1H, aryl, *J* = 7.8 Hz); 7.13–7.15 (m, 1H aryl); 7.34–7.38 (m, 2H, aryl); 7.46 (t, 2H, aryl, *J* = 7.5 Hz); 7.52 (d, 2H, aryl, *J* = 8.2 Hz); 7.59–7.64 (m, 2H, aryl); 7.93 (d, 1H, aryl, *J* = 8.0 Hz); 8.43 (t, 1H, aryl, *J* = 5.6 Hz); 10.9 (s, 1H, N*H*). HR-MS *m/z* calcd for $C_{34}H_{39}N_4O_4$ $[(M + H)]^+$: 567.2966; found 567.2958.

6.1.5.12. tert-butyl ((S)-1-(((S)-1-(([1,1'-biphenyl]-4-ylmethyl) amino)-3-(1H-indol-3-yl)-1-oxopropan-2-yl)amino)-1-oxopent-4-yn-2-yl)carbamate (12). Compound **12** was synthesized in 82% yield starting from intermediate **5** and Boc-L-Pra-OH following the general procedure **A**. FC in n-hexane/ethyl acetate 3/1, Rf = 0.45. White powder. ^{1}H NMR (400 MHz, CD_3OD): *δ*: 1.32 (s, 9H, C*H*$_3$); 2.35 (s, 1H, C*H*); 2.54–2.65 (m, 2H, C*H*$_2$); 3.27–3.37 (m, 2H, C*H*$_2$); 4.15 (t, 1H, C*H*, *J* = 6.2 Hz); 4.25–4.37 (m, 2H, C*H*$_2$); 4.73 (t, 1H, C*H*, *J* = 6.0 Hz); 7.04–7.15 (m, 4H, aryl); 7.33 (t, 1H, aryl, *J* = 7.4 Hz); 7.37–7.47 (m, 6H, aryl); 7.58 (d, 2H, aryl, *J* = 9.2 Hz); 7.65 (d, 1H, aryl, *J* = 7.6 Hz). HR-MS *m/z* calcd for $C_{34}H_{37}N_4O_4$ $[(M + H)]^+$: 565.2809; found 565.2815.

6.1.5.13. tert-butyl ((S)-1-(((S)-1-(benzylamino)-3-(1H-indol-3-yl)-1-oxopropan-2-yl)amino)-1-oxopent-4-en-2-yl)carbamate (13). Obtained from coupling reaction (procedure **A**) between **6** and Boc-L-allylgly-OH. FC in hexane/ethyl acetate 2/1, Rf = 0.40. White powder (78% yield). ^{1}H NMR (400 MHz, CD_3OD): *δ*: 1.27 (s, 9H, C*H*$_3$); 2.25–2.34 (m, 1H, C*H*$_{2a}$); 2.44–2.48 (m, 1H, C*H*$_{2b}$); 3.28 (d, 2H, C*H*, *J* = 4.6 Hz); 4.02 (t, 1H, C*H*, *J* = 5.2 Hz); 4.21–4.26 (m, 1H, C*H*$_{2a}$); 4.32 (dd, 1H, C*H*$_{2b}$, *J'* = 3.4, *J"* = 11.9 Hz); 4.70 (t, 1H, C*H*, *J* = 4.5 Hz); 5.04–5.11 (m, 2H, C*H*$_2$); 5.67–5.75 (m, 1H, C*H*); 7.03–7.10 (m, 5H, aryl); 7.14 (t, 1H, aryl, *J* = 5.6 Hz); 7.20–7.25 (m, 2H, aryl); 7.38 (d, 1H, aryl, *J* = 6.5 Hz); 7.63 (d, 1H, aryl, *J* = 6.2 Hz). HR-MS *m/z* calcd for $C_{28}H_{35}N_4O_4$ $[(M + H)]^+$: 491.2653; found 491.2661.

6.1.5.14. tert-butyl ((S)-1-(((S)-1-(benzylamino)-3-(1H-indol-3-yl)-1-oxopropan-2-yl)amino)-4-methyl-1-oxopentan-2-yl)carbamate (14). The intermediate **14** was obtained using L-Boc-Leu-OH and **6** as starting material, following general procedure **A**. FC in hexane/ethyl acetate 2/1, Rf = 0.45. White powder (77% yield). ^{1}H NMR (400 MHz, DMSO): *δ*: 0.79 (d, 3H, C*H*$_3$, *J* = 6.4 Hz); 0.83 (d, 3H, C*H*$_3$, *J* = 6.5 Hz); 1.24–1.35 (m, 12H, C*H*, C*H*$_2$, C*H*$_3$); 3.01–3.15 (m, 2H, C*H*$_2$); 3.90–3.96 (m, 1H, C*H*); 4.22 (d, 2H, C*H*$_2$, *J* = 5.6 Hz); 4.59 (q, 1H, CH, *J* = 6.9 Hz); 6.97 (t, 1H, aryl, *J* = 6.9 Hz); 7.04–7.11 (m, 3H, aryl); 7.18–7.25 (m, 3H, aryl); 7.33 (d, 1H, aryl, *J* = 8.0 Hz); 7.57 (d, 1H, aryl, *J* = 7.7 Hz); 7.81 (d, 1H, aryl, *J* = 8.0 Hz); 8.40 (t, 1H, N*H*, *J* = 5.1 Hz); 10.82 (s, 1H, N*H*). HR-MS *m/z* calcd for $C_{29}H_{38}N_4O_4$ $[(M + H)]^+$: 506.2888; found 506.2899.

6.1.5.15. 2-Amino-N-(1-(tert-butylamino)-3-(1H-indol-3-yl)-1-oxopropan-2-yl)-3-phenylpropanamide (15). Intermediate **15** was synthesized according to the general procedure **B**, starting from **8**. White powder (95% yield). FC in hexane/ethyl acetate 7/3, Rf: 0.47. Yellow oil (55% yield). ^{1}H NMR (400 MHz, $CDCl_3$): *δ*: 1.17 (s, 9H, C*H*$_3$); 2.71 (dd, 1H, C*H*$_{2a}$ *J'* = 8.3, *J"* = 13.6 Hz); 3.06 (dd, 1*H*, C*H*$_{2b}$ *J'* = 8.0, *J"* = 14.5 Hz); 3.13 (dd, 1H, C*H*$_{2a}$ *J'* = 4.9, *J"* = 13.8 Hz); 3.23 (dd, 1H, C*H*$_{2b}$, *J'* = 6.5, *J"* = 14.6 Hz); 3.73 (t, 1H, C*H*, *J* = 5.3 Hz); 4.62 (q, 1H, C*H*, *J* = 7.6 Hz); 5.63 (bs, 1H, N*H*); 7.05 (s, 1H, aryl); 7.11–7.30 (m, 6H, aryl); 7.35 (d, 1H, aryl, *J* = 8.0 Hz); 7.68 (d, 1H, aryl, *J* = 8.0 Hz); 7.88 (d, 1H, aryl, *J* = 7.1 Hz); 8.29 (bs, 1H, N*H*). HR-MS *m/z* calcd for $C_{24}H_{31}N_4O_2$ $[(M + H)]^+$: 407.2442; found 407.2451.

6.1.5.16. 2-Amino-N-(1-(tert-butylamino)-3-(1H-indol-3-yl)-1-oxopropan-2-yl)-4-methylpentanamide (16). Intermediate **16** was synthesized according to the general procedure **B**, starting from **9**. White powder (94% yield). ^{1}H NMR (400 MHz, CD_3OD): *δ*: 0.91 (d, 3H, C*H*$_3$, *J* = 6.5 Hz); 0.94 (d, 3H, C*H*$_3$, *J* = 6.5 Hz); 1.39–1.48 (m, 1H, C*H*$_{2a}$); 1.54–1.61 (m, 1H, C*H*$_{2b}$); 1.65–1.71 (m, 1H, C*H*); 3.24 (dd, 1H, C*H*$_{2a}$ *J'* = 7.8, *J"* = 14.7 Hz); 3.34 (dd, 1H, C*H*$_{2b,}$ *J'* = 5.5, *J"* = 14.7 Hz); 3.56 (dd, 1H, C*H*, *J'* = 6.0, *J"* = 8.4 Hz); 7.03 (t, 1H, aryl, *J* = 7.9 Hz); 7.11 (t, 1H, aryl, *J* = 8.1 Hz); 7.13 (s, 1H, aryl); 7.37 (d, 1H, aryl, *J* = 8.1 Hz); 7.55 (d, 1H, aryl, *J* = 7.9 Hz). HR-MS *m/z* calcd for $C_{21}H_{33}N_4O_2$ $[(M + H)]^+$: 373.2598; found 373.2604.

6.1.5.17. tert-butyl ((S)-1-(((S)-1-(tert-butylamino)-3-(1H-indol-3-yl)-1-oxopropan-2-yl)amino)-1-oxopent-4-yn-2-yl)carbamate (17). Intermediate **17** was synthesized according to the general procedure **B**, starting from **10**. White powder (92% yield). ^{1}H NMR (400 MHz, $CDCl_3$): *δ*: 1.15 (s, 9H, C*H*$_3$); 1.96 (t, 1H, C*H*, *J* = 2.6 Hz); 2.47–2.54 (m, 1H, C*H*$_{2a}$); 2.62–2.68 (m, 1H, C*H*$_{2b}$); 3.12 (dd, 1H, C*H*$_{2a}$, *J'* = 8.3, *J"* = 14.4 Hz); 3.30 (dd, 1H, C*H*$_{2b}$ *J'* = 6.7, *J"* = 15.0 Hz); 3.49 (dd, 1H, C*H*, *J'* = 4.6, *J"* = 7.1 Hz); 4.63 (q, 1H, C*H*, *J* = 8.1 Hz); 5.57 (bs, 1H, N*H*); 7.07 (s, 1H, aryl); 7.14 (t, 1H, aryl, *J* = 7.2 Hz); 7.21

(t, 1H, aryl, $J = 7.0$ Hz); 7.37 (d, 1H, aryl, $J = 8.0$ Hz); 7.74 (d, 1H, aryl, $J = 7.8$ Hz); 8.49 (bs, 1H, N*H*). HR-MS *m/z* calcd for $C_{20}H_{27}N_4O_2$ $[(M + H)]^+$: 355.2129; found 355.2136.

6.1.5.18. (S)−N-((S)-1-(([1,1′-biphenyl]-4-ylmethyl)amino)-3-(1H-indol-3-yl)-1-oxopropan-2-yl)-2-aminopent-4-enamide (18). Intermediate **18** was synthesized according to the general procedure **B**, starting from **11**. White powder (89% yield). ^{1}H NMR (400 MHz, CD_3OD): δ: 1.95−2.03 (m, 1H, CH_{2a}); 2.33−2.38 (m, 1H, CH_{2b}); 3.18−3.21 (m, 1H, C*H*); 3.26−3.35 (m, 2H, CH_2); 4.28−4.40 (m, 2H, CH_2); 4.93−5.04 (m, 3H, CH_2 and C*H*); 5.45−5.55 (m, 1H, C*H*); 6.94 (s, 1H, aryl); 7.06−7.11 (m, 3H, aryl); 7.19 (t, 1H, aryl, $J = 7.7$ Hz); 7.34−7.39 (m, 3H, aryl); 7.43−7.47 (m, 4H aryl); 7.56 (d, 1H, aryl, $J = 7.2$ Hz); 7.68 (d, 1H, aryl, $J = 8.0$ Hz); 8.14 (d, 1H, N*H*, $J = 8.2$ Hz); 8.95 (s, 1H, N*H*). HR-MS *m/z* calcd for $C_{29}H_{31}N_4O_2$ $[(M + H)]^+$: 467.2442; found 467.2436.

6.1.5.19. (S)−N-((S)-1-(([1,1′-biphenyl]-4-ylmethyl)amino)-3-(1H-indol-3-yl)-1-oxopropan-2-yl)-2-aminopent-4-ynamide (19). Intermediate **19** was synthesized according to the general procedure **B**, starting from **12**. White powder (95% yield). ^{1}H NMR (400 MHz, CD_3OD): δ: 2.49 (s, 1H, C*H*); 2.66 (dd, 1H, CH_{2a}, $J' = 7.2$, $J'' = 14.8$ Hz); 2.75 (dd, 1H, CH_{2b}, $J' = 5.1$, $J'' = 19.7$ Hz); 3.21 (dd, 1H, CH_{2a}, $J' = 6.9$, $J'' = 14.4$ Hz); 3.29−3.36 (m, 1H, CH_{2b}); 3.83 (t, 1H, C*H*, $J = 5.4$ Hz); 4.25 (d, 1H, CH_{2a}, $J = 15.0$ Hz); 4.37 (d, 1H, CH_{2b}, $J = 15.0$ Hz); 4.78 (t, 1H, C*H*, $J = 7.3$ Hz); 7.03−7.15 (m, 4H aryl); 7.35 (t, 1H, aryl, $J = 7.6$ Hz); 7.37−7.49 (m, 6H, aryl); 7.58 (d, 2H, aryl, $J = 9.2$ Hz); 7.66 (d, 1H, aryl, $J = 7.6$ Hz). HR-MS *m/z* calcd for $C_{29}H_{29}N_4O_2$ $[(M + H)]^+$: 465.2285; found 465.2292.

6.1.5.20. (S)-2-Amino-N-((S)-1-(benzylamino)-3-(1H-indol-3-yl)-1-oxopropan-2-yl)pent-4-enamide (20). Intermediate **20** was synthesized according to the general procedure **B**, starting from **13**. White powder (93% yield). ^{1}H NMR (400 MHz, CD_3OD): δ: 2.55−2.61 (m, 1H, CH_{2a}); 2.65−2.69 (m, 1H, CH_{2b}); 3.19 (dd, 1H, CH_{2a}, $J' = 5.5$, $J'' = 11.3$ Hz); 3.31 (dd, 1H, CH_{2b}, $J' = 6.3$, $J'' = 10.9$ Hz); 3.95 (t, 1H, C*H*, $J = 5.5$ Hz); 4.25 (dd, 1H, CH_{2a}, $J' = 3.7$, $J'' = 11.8$ Hz); 4.31 (dd, 1H, CH_{2b}, $J' = 4.4$, $J'' = 12.0$ Hz); 4.77 (t, 1H, C*H*, $J = 6.0$ Hz); 5.21−5.27 (m, 2H, CH_2); 5.72−5.80 (m, 1H, C*H*); 7.02−7.07 (m, 3H, aryl); 7.14 (t, 1H, aryl, $J = 5.7$ Hz); 7.21−7.26 (m, 4H, aryl); 7.39 (d, 1H, aryl, $J = 6.4$ Hz); 7.66 (d, 1H, aryl, $J = 6.3$ Hz). HR-MS *m/z* calcd for $C_{23}H_{27}N_4O_2$ $[(M + H)]^+$: 391.2129; found 391.2135.

6.1.5.21. (S)-2-Amino-N-((S)-1-(benzylamino)-3-(1H-indol-3-yl)-1-oxopropan-2-yl)-4-methylpentanamide (21). Intermediate **21** was synthesized according to the general procedure **B**, starting from **14**. White powder (95% yield). ^{1}H NMR (400 MHz, CD_3OD): δ: 0.87 (d, 3H, CH_3, $J = 6.6$ Hz); 0.90 (d, 3H, CH_3, $J = 6.5$ Hz); 1.20−1.28 (m, 1H, CH_{2a}); 1.38−1.46 (m, 1H, CH_{2b}); 1.56−1.67 (m, 1H, C*H*); 3.27−3.37 (m, 3H, C*H* and CH_2); 4.25 (d, 1H, CH_{2a}, $J = 15.0$ Hz); 4.32 (d, 1H, CH_{2b}, $J = 15.0$ Hz); 4.72 (t, 1H, C*H*, $J = 7.2$ Hz); 7.01−7.13 (m, 6H, aryl); 7.20−7.26 (m, 2H, aryl); 7.36 (d, 1H, aryl, $J = 8.1$ Hz); 7.64 (d, 1H, aryl, $J = 7.8$ Hz). HR-MS *m/z* calcd for $C_{24}H_{31}N_4O_2$ $[(M + H)]^+$: 407.2442; found 407.2435.

6.1.5.22. (S)-2-(([1,1′-biphenyl]-4-ylmethyl)amino)-N-((S)-1-(tert-butylamino)-3-(1H-indol-3-yl)-1-oxopropan-2-yl)-3-phenylpropanamide (22). Final product **22** was synthesized in 64% yield starting from **15** and 4-phenylbenzaldehyde, following the general procedure **C**. FC in hexane/ethyl acetate 1/1, Rf = 0.35. Yellowish powder. ^{1}H NMR (400 MHz, $CDCl_3$): δ: 1.18 (s, 9H, CH_3); 2.61 (dd, 1H, CH_{2a}, $J' = 9.3$, $J'' = 13.8$ Hz); 3.11−3.17 (m, 2H, CH_{2b} and CH_{2a}); 3.34−3.44 (m, 3H, C*H*, CH_{2b} and CH_{2a}); 3.53, (d, 1H, CH_{2a}, $J = 13.4$ Hz); 3.70 (d, 1H, CH_{2b}, $J = 13.6$ Hz); 4.69 (dd, 1H, C*H*, $J' = 8.1$, $J'' = 14.3$ Hz); 5.59 (bs, 1H, N*H*); 7.06 (d, 3H, aryl, $J = 8.1$ Hz); 7.12−7.30 (m, 6H, aryl); 7.39 (t, 2H, aryl, $J = 8.1$ Hz); 7.44−7.48 (m, 4H, aryl); 7.58 (d, 2H, aryl, $J = 8.4$ Hz); 7.76 (d, 1H, aryl, $J = 7.8$ Hz); 8.07 (d, 1H, aryl, $J = 5.8$ Hz); 8.39 (bs, 1H, N*H*). ^{13}C NMR (100 MHz, $CDCl_3$) δ 28.2,28.5, 39.0, 51.1, 52.1, 54.0, 63.0, 111.21, 111.28, 119.2, 119.8, 122.3, 123.2, 127.0, 127.3, 127.5, 128.5, 128.8, 1292, 136.3, 137.2, 138.1, 140.1, 140.9. HR-MS *m/z* calcd for $C_{37}H_{40}N_4O_2$ $[(M + H)]^+$: 573.3230; found 573.3238.

6.1.5.23. 2-(([1,1′-biphenyl]-4-ylmethyl)amino)-N-(1-(tert-butylamino)-3-(1H-indol-3-yl)-1-oxopropan-2-yl)-4-methylpentanamide (23). Obtained from **16** and 4-phenylbenzaldehyde following the general procedure **C**. FC in hexane/ethyl acetate 1/1, Rf = 0.35. Yellowish powder (56% yield). ^{1}H NMR (400 MHz, $CDCl_3$): δ: 0.74 (d, 3H, CH_3, $J = 6.4$ Hz); 0.81 (d, 3H, CH_3, $J = 6.4$ Hz); 1.16−1.24 (m, 1H, C*H*); 1.40−1.45 (m, 1H, CH_{2a}); 1.47−1.56 (m, 1H, CH_{2b}); 3.07 (dd, 1H, CH_{2a}, J' = 8.0, J" = 14.4 Hz); 3.17−3.20 (m, 1H, C*H*); 3.24 (dd, 1H, CH_{2b}, $J' = 6.5$, $J'' = 14.5$ Hz); 3.54 (d, 1H, CH_{2a}, $J = 12.9$ Hz); 4.59 (q, 1H, C*H*); 5.54 (bs, 1H, N*H*); 7.03 (s, 1H, aryl); 7.06 (t, 1H, aryl, $J = 7.7$ Hz); 7.13 (t, 1H, aryl, $J = 7.2$ Hz); 7.18−7.21 (m, 2H, aryl); 7.27 (d, 1H, aryl, $J = 8.3$ Hz); 7.35 (t, 2H, aryl, $J = 7.5$ Hz); 7.43−7.49 (m, 4H, aryl); 7.69 (d, 1H, aryl, $J = 7.7$ Hz); 7.85 (d, 1H, aryl, $J = 7.9$ Hz); 8.06 (s, 1H, N*H*). ^{13}C NMR (100 MHz, $CDCl_3$) δ 25.0, 28.2, 28.5, 29.7, 42.4, 51.2, 52.1, 54.0, 60.8, 111.2, 111.4, 119.2, 119.8, 122.3, 123.1, 127.1, 127.3, 128.8, 129.0, 136.3, 140.4, 140.8, 170.2. HR-MS *m/z* calcd for $C_{34}H_{43}N_4O_2$ $[(M + H)]^+$: 539.3381; found 539.3390.

6.1.5.24. (S)-2-(([1,1′-biphenyl]-4-ylmethyl)amino)-N-((S)-1-(tert-butylamino)-3-(1H-indol-3-yl)-1-oxopropan-2-yl)pent-4-ynamide (24). Synthesized according to the general procedure **C**, starting from intermediate **17** and 4-phenylbenzaldehyde. FC in hexane/ethyl acetate 1/1, Rf = 0.30. White powder (57% yield). ^{1}H NMR (400 MHz, $CDCl_3$): δ: 1.24 (s, 9H, CH_3); 2.32 (s, 1H, C*H*); 2.43−2.58 (m, 2H, CH_2); 3.17−3.26 (m, 2H, CH_2); 3.32−3.34 (m, 1H, C*H*); 3.55 (dd, 2H, CH_2, J' = 13.2, J" = 15.2 Hz); 4.69 (t, 1H, CH, $J = 7.3$ Hz); 7.03 (t, 1H, aryl, $J = 7.9$ Hz); 7.11 (t, 1H, aryl, $J = 7.9$ Hz); 7.14 (s, 1H, aryl); 7.23 (d, 2H, aryl, $J = 8.2$ Hz); 7.33 (d, 2H, aryl, $J = 8.9$ Hz); 7.42 (t, 2H, aryl, $J = 7.4$ Hz); 7.49 (d, 2H, aryl, $J = 8.2$ Hz); 7.58 (d, 2H, aryl, $J = 7.2$ Hz); 7.68 (d, 1H, aryl, $J = 7.6$ Hz). ^{13}C NMR (100 MHz, $CDCl_3$) δ 21.7, 27.4, 28.0, 50.8, 54.2, 58.1, 59.6, 71.1, 79.2, 109.5, 110.9, 118.3, 121.1, 123.3, 126.5, 126.8, 127.5, 128.6, 136.7, 138.2, 139.9, 140.8, 171.3, 173.2. HR-MS *m/z* calcd for $C_{33}H_{37}N_4O_2$ $[(M + H)]^+$: 521.2911; found 521.2918.

6.1.5.25. (S)-2-(([1,1′-biphenyl]-4-ylmethyl)amino)-N-((S)-1-(benzylamino)-3-(1H-indol-3-yl)-1-oxopropan-2-yl)-4-methylpentanamide (25). Synthesized according to the general procedure **C**, starting from intermediate **21** and 4-phenylbenzaldehyde. FC in hexane/ethyl acetate 1/1, Rf = 0.48. White powder (60% yield). ^{1}H NMR (400 MHz, CD_3OD): δ: 0.78 (d, 3H, CH_3, $J = 6.6$ Hz); 0.88 (d, 3H, CH_3, $J = 6.6$ Hz); 1.28−1.40 (m, 2H, CH_2); 1.56−1.63 (m, 1H, C*H*); 3.13 (t, 1H, C*H*, $J = 6.8$ Hz); 3.21 (dd, 1H, CH_{2a}, $J' = 7.9$, $J'' = 14.5$ Hz); 3.28 (dd, 1H, CH_{2b}, $J' = 6.6$, $J'' = 14.6$ Hz); 3.48 (dd, 2H, CH_2, $J' = 13.1$, $J'' = 25.1$ Hz); 4.26 (d, 1H, CH_{2a}, $J = 15.0$ Hz); 4.36 (d, 1H, CH_{2b}, $J = 15.0$ Hz); 4.82 (t, 1H, C*H*, $J = 7.8$ Hz); 7.03−7.14 (m, 6H, aryl); 7.17−7.27 (m, 5H, aryl); 7.31−7.36 (m, 1H, aryl); 7.41−7.47 (m, 4H, aryl); 7.57 (d, 2H, aryl, $J = 8.5$ Hz); 7.67 (d, 1H, aryl, $J = 7.8$ Hz). ^{13}C NMR (100 MHz, CD_3OD) δ 21.3, 21.9, 24.5, 27.9, 42.5, 42.7, 51.2, 53.7, 60.0, 109.4, 111.0, 118.2, 118.5, 121.1, 123.3, 126.5, 126.7, 126.84, 127.04, 128.1, 128.4, 128.7, 136.7, 138.1, 138.4, 139.8, 140.8, 172.4, 175.9. HR-MS *m/z* calcd for $C_{37}H_{40}N_4O_2$ $[(M + H)]^+$: 573.3224; found 573.3230.

6.1.5.26. (S)−N-((S)-1-(([1,1′-biphenyl]-4-ylmethyl)amino)-3-(1H-indol-3-yl)-1-oxopropan-2-yl)-2-(benzylamino)pent-4-enamide (26). Final product **26** was synthesized as a yellow powder in 66% yield

starting from **18** and benzaldehyde and following the general procedure **C**. FC in hexane/ethyl acetate 1/1, Rf = 0.45. ^{1}H NMR (400 MHz, CD_3OD): δ: 2.19–2.31 (m, 2H, CH_2); 3.07 (dd, 1H, CH_{2a}, $J' = 8.3$, $J'' = 14.4$ Hz); 3.18–3.23 (m, 4H, CH_{2b}, CH_2 and C*H*); 4.25 (q, 2H, CH_2, $J = 15.0$ Hz); 4.73–4.76 (m, 1H, C*H*); 4.88–4.94 (m, 2H, CH_2); 5.47–5.57 (m, 1H, C*H*); 6.93–7.02 (m, 7H aryl); 7.07 (d, 2H, aryl, $J = 8.2$ Hz); 7.14 (d, 2H, aryl, $J = 2.8$ Hz); 7.21 (t, 1H, aryl, $J = 6.8$ Hz); 7.30 (t, 2H, aryl, $J = 7.4$ Hz); 7.38 (d, 2H, aryl, $J = 8.2$ Hz); 7.45 (d, 2H, aryl, $J = 7.2$ Hz); 7.57 (d, 1H, aryl, $J = 7.6$ Hz). ^{13}C NMR (100 MHz, CD_3OD) δ 28.1, 36.4, 42.4, 50.9, 54.0, 60.2, 109.4, 111.1, 118.09, 118.20, 118.6, 121.2, 123.4, 126.49, 126.66, 126.91, 127.6, 128.23, 128.43, 128.7, 132.5, 136.7, 137.2, 140.0, 140.7, 172.1. HR-MS *m/z* calcd for $C_{36}H_{37}N_4O_2$ $[(M + H)]^+$: 557.2911; found 557.2918.

6.1.5.27. (S)–N-((S)-1-(([1,1′-biphenyl]-4-ylmethyl)amino)-3-(1H-indol-3-yl)-1-oxopropan-2-yl)-2-(benzylamino)pent-4-ynamide (27). Final product **27** was synthesized in 68% yield starting from **19** and benzaldehyde, following the general procedure **C**. FC in hexane/ethyl acetate 1/1, Rf = 0.40. White powder (55% yield). ^{1}H NMR (400 MHz, CD_3OD): δ: 2.54 (s, 1H, C*H*); 2.79 (dd, 2H, CH_2, $J' = 2.7$, $J'' = 6.5$ Hz); 3.17 (dd, 1H, CH_{2a}, $J' = 9.4$, $J'' = 14.5$ Hz); 3.38 (dd, 1H, CH_{2b}, $J' = 6.2$, $J'' = 14.8$ Hz); 3.43 (d, 1H, CH_{2a}, $J = 13.0$ Hz); 3.63 (d, 1H, CH_{2b}, $J = 13.0$ Hz); 3.83 (t, 1H, C*H*, $J = 6.5$ Hz); 4.42 (q, 2H, CH_2, $J = 15.0$ Hz); 5.01 (dd, 1H, C*H*, $J' = 6.0$, $J'' = 9.4$ Hz); 7.06–7.09 (m, 2H aryl); 7.13 (d, 2H, aryl, $J = 7.0$ Hz); 7.19 (s, 1H, aryl); 7.23–7.26 (m, 3H, aryl); 7.38–7.46 (m, 6H, aryl); 7.55 (d, 2H, aryl, $J = 8.2$ Hz); 7.60 (d, 2H, aryl, $J = 7.2$ Hz); 7.73–7.76 (m, 1H, aryl). ^{13}C NMR (100 MHz, CD_3OD) δ 20.3, 28.3, 42.4, 49.8, 54.4, 57.7, 73.8, 109.5, 111.2, 118.2, 118.6, 121.2, 123.5, 126.5, 126.7, 127.0, 127.4, 127.7, 128.4, 128.8, 129.4, 129.8, 130.3, 136.7, 137.2, 140.1, 140.7, 165.7, 171.6. HR-MS *m/z* calcd for $C_{36}H_{34}N_4O_2$ $[(M + H)]^+$: 555.2755; found 555.2763.

6.1.5.28. (S)–N-((S)-1-(([1,1′-biphenyl]-4-ylmethyl)amino)-3-(1H-indol-3-yl)-1-oxopropan-2-yl)-2-(propylamino)pent-4-ynamide (28). Final product **28** was synthesized in 64% starting from **19** and propionaldehyde following the general procedure **C**. FC in hexane/ethyl acetate 1/2, Rf = 0.35. White powder. ^{1}H NMR (400 MHz, CD_3OD): δ: 0.95 (t, 3H, CH_3, $J = 7.4$ Hz); 1.36–1.42 (m, 2H, CH_2); 1.54–1.58 (m, 2H, CH_2); 2.60 (s, 1H, C*H*); 2.80 (dd, 1H, CH_{2a}, $J' = 7.4$, $J'' = 17.5$ Hz); 2.88 (dd, 1H, CH_{2b}, $J' = 8.1$, $J'' = 17.5$ Hz); 3.20 (dd, 1H, CH_{2a}, $J' = 7.0$, $J'' = 14.3$ Hz); 3.31–3.37 (m, 1H, CH_{2b}); 4.05 (dd, 1H, C*H*, $J' = 5.4$, $J'' = 7.4$ Hz); 4.25 (d, 1H, CH_{2a}, $J = 15.1$ Hz); 4.36–4.40 (m, 1H, CH_{2b}); 4.78–4.80 (m, 1H, C*H*); 7.03–7.15 (m, 4H aryl); 7.34 (t, 1H, aryl, $J = 7.4$ Hz); 7.38–7.48 (m, 6H, aryl); 7.58 (d, 2H, aryl, $J = 8.5$ Hz); 7.67 (d, 1H, aryl, $J = 7.9$ Hz). ^{13}C NMR (100 MHz, CD_3OD) δ 12.8, 21.1, 27.9, 34.4, 42.4, 51.4, 54.8, 73.7, 104.5, 109.1, 111.0, 118.0, 118.5, 121.2, 123.4, 126.5, 126.9, 127.3, 127.5, 128.4, 136.7, 139.9, 140.7, 167.0, 171.8. HR-MS *m/z* calcd for $C_{32}H_{35}N_4O_2$ $[(M + H)]^+$: 507.2755; found 507.2747.

6.1.5.29. (S)–N-((S)-1-(benzylamino)-3-(1H-indol-3-yl)-1-oxopropan-2-yl)-2-(2-chloroacetamido)pent-4-enamide (29). Intermediate **20** (1 mmol) was dissolved in THF and added with TEA (1.2 eq), and chloro acetylchloride (1.2 eq). The mixture was allowed to react for 20 min. Afterward, the reaction mixture was diluted with dichloromethane (20 mL), and the resulting solution was washed successively with water (2 × 25 mL), dried over Na_2SO_4 and evaporated to dryness. The crude products were purified by flash chromatography using n-hexane/ethyl acetate 1/1, Rf = 0.38. White powder (62% yield). ^{1}H NMR (400 MHz, DMSO): δ: 2.24–2.31 (m, 1H, CH_{2a}); 2.37–2.44 (m, 1H, CH_{2b}); 2.99 (dd, 1H, CH_{2a}, $J' = 8.1$, $J'' = 14.5$ Hz); 3.15 (dd, 1H, CH_{2b}, $J' = 4.6$, $J'' = 14.5$ Hz); 4.09 (dd, 2H, CH_2, $J' = 13.1$, $J'' = 15.8$ Hz); 4.24–4.26 (m, 2H, CH_2); 4.38–4.45 (m, 1H, C*H*); 4.56–4.61 (m, 1H, C*H*); 5.00 (dd, 2H, CH_2, $J' = 17.2$, $J'' = 25.5$ Hz); 5.61–5.71 (m, 1H, C*H*); 6.98 (t, 1H, aryl, $J = 7.8$ Hz); 7.06 (t, 1H, aryl, $J = 7.0$ Hz); 7.10–7.13 (m, 2H, aryl); 7.19–7.28 (m, 3H, aryl); 7.34 (d, 1H, aryl, $J = 8.1$ Hz); 8.25 (d, 1H, aryl, $J = 8.0$ Hz); 8.40 (t, 1H, aryl, $J = 5.9$ Hz); 10.83 (s, 1H, N*H*). ^{13}C NMR (100 MHz, DMSO) δ 28.3, 36.9, 40.5, 42.5, 43.0, 52.7, 54.1, 110.3, 111.7, 118.1, 118.9, 121.3, 124.1, 127.1, 127.4, 127.8, 128.6, 134.3, 136.5, 139.6, 166.1, 170.7, 171.6. HR-MS *m/z* calcd for $C_{25}H_{27}ClN_4O_3$ $[(M + H)]^+$: 467.1844; found 467.1852.

6.1.5.30. Methyl 1-isobutyl-1H-indole-5-carboxylate (30). Intermediate **30** was obtained according to the general procedure **D**, starting from methyl indole-5-carboxylate and 1-iodo-2-methylpropane, as previously described [31]. FC in n-hexane/ethyl acetate 3/1, Rf = 0.4. Yellowish oil (80% yield). ^{1}H NMR (400 MHz, $CDCl_3$): δ: 0.94 (d, 6H, CH_3, $J = 6.7$ Hz); 2.17–2.24 (m, 1H, C*H*); 3.93 (d, 2H, CH_2, $J = 7.3$ Hz); 3.96 (s, 3H, CH_3); 6.61 (d, 1H, aryl, $J = 3.2$ Hz); 7.14 (d, 1H, aryl, $J = 3.1$ Hz); 7.35 (d, 1H, aryl, $J = 8.7$ Hz); 7.94 (d, 1H, aryl, $J = 10.1$ Hz); 8.44 (s, 1H, aryl). HR-MS *m/z* calcd for $C_{14}H_{18}NO_2$ $[(M + H)]^+$: 232.1332; found 232.1340.

6.1.5.31. Methyl 1-methyl-1H-indole-5-carboxylate (31). Intermediate **31** was obtained according to the general procedure **D**, starting from methyl indole-5-carboxylate and iodomethane, as previously described [30]. FC in n-hexane/ethyl acetate 3/1, Rf = 0.4. Yellowish oil (82% yield). ^{1}H NMR (400 MHz, $CDCl_3$): δ: 3.85 (s, 3H, CH_3); 3.92 (s, 3H, CH_3); 6.57 (d, 1H, aryl, $J = 3.4$ Hz); 7.26 (d, 1H, aryl, $J = 3.4$ Hz); 7.43 (d, 1H, aryl, $J = 9.2$ Hz); 7.87 (d, 1H, aryl, $J = 9.6$ Hz); 8.32 (s, 1H, aryl). HR-MS *m/z* calcd for $C_{11}H_{12}NO_2$ $[(M + H)]^+$: 190.0863; found 190.0871.

6.1.5.32. Methyl 3-((([1,1′-biphenyl]-4-ylmethyl)amino)methyl)-1-isobutyl-1H-indole-5-carboxylate (32). The compound **32** was obtained using general procedure **E**, starting from intermediate **30** which was reacted with 2-([1,1′-biphenyl]-4-yl)ethan-1-amine. FC in dichloromethane/methanol 4.8/0.2. Rf = 0.42. Yellowish oil (70% yield). ^{1}H NMR (400 MHz, $CDCl_3$): δ: 3.83 (s, 3H, CH_3); 3.86 (s, 2H, CH_2); 3.93 (s, 3H, CH_3); 3.99 (s, 2H, CH_2); 7.28 (s, 1H, aryl); 7.32–7.38 (m, 5H, aryl); 7.43 (d, 1H, aryl, $J = 8.8$ Hz); 7.88 (d, 1H, aryl, $J = 9.2$ Hz); 8.35 (s, 1H, aryl). HR-MS *m/z* calcd for $C_{28}H_{31}N_2O_2$ $[(M + H)]^+$: 427.2380; found 427.2389.

6.1.5.33. Methyl 3-(((2-([1,1′-biphenyl]-4-yl)ethyl)amino)methyl)-1-isobutyl-1H-indole-5-carboxylate (33). The compound **33** was obtained using general procedure **E**, starting from intermediate **31** which was reacted with benzylamine. FC in dichloromethane/methanol 4.8/0.2. Rf = 0.45. Yellowish oil (75% yield). ^{1}H NMR (400 MHz, $CDCl_3$): δ: 0.94 (d, 6H, CH_3, $J = 6.6$ Hz); 2.14–2.25 (m, 1H, C*H*); 2.94 (t, 2H, CH_2, $J = 7.3$ Hz); 3.06 (t, 2H, CH_2, $J = 6.9$ Hz); 3.89 (d, 2H, CH_2, $J = 7.3$ Hz); 3.94 (s, 3H, CH_3); 4.09 (s, 2H, CH_2); 7.10 (s, 1H, aryl); 7.31–7.33 (m, 4H, aryl); 7.36 (d, 1H, aryl, $J = 7.4$ Hz); 7.45 (t, 2H, aryl, $J = 7.8$ Hz); 7.55 (d, 2H, aryl, $J = 8.2$ Hz); 7.60 (d, 2H, aryl, $J = 8.9$ Hz); 7.94 (d, 1H, aryl, $J = 10.1$ Hz); 8.43 (s, 1H, N*H*). HR-MS *m/z* calcd for $C_{29}H_{33}N_2O_2$ $[(M + H)]^+$: 441.2537; found 441.2549.

6.1.5.34. Methyl 3-((([1,1′-biphenyl]-4-ylmethyl)(benzyl)amino)methyl)-1-isobutyl-1H-indole-5-carboxylate (34). Final compound **34** was obtained following general procedure **C**, using as starting materials intermediate **32** and benzaldehyde. FC in dichloromethane/methanol 4.8/0.2. Rf = 0.27. Yellowish oil (78% yield). ^{1}H NMR (400 MHz, $CDCl_3$): δ: 0.94 (d, 6H, CH_3, $J = 6.7$ Hz); 2.15–2.25 (m, 1H, C*H*); 2.86–2.89 (m, 2H, CH_2); 2.94–2.98 (m, 2H, CH_2); 3.80 (s, 2H, CH_2); 3.89 (d, 2H, CH_2, $J = 7.4$ Hz); 3.94 (s, 2H, CH_2); 3.99 (s, 3H, CH_3); 7.02 (s, 1H, aryl); 7.23 (d, 2H, aryl, $J = 8.1$ Hz); 7.28–7.41 (m, 5H, aryl); 7.45–7.53 (m, 6H, aryl); 7.64 (d, 2H, aryl, $J = 7.1$ Hz); 7.98 (d, 1H, aryl, $J = 8.7$ Hz); 8.54 (s, 1H, aryl). ^{13}C NMR (100 MHz,

$CDCl_3$) δ 203, 29.7, 33.2, 49.2, 51.8, 54.1, 55.2, 58.6, 65.9, 109.2, 114.0, 120.8, 123.0, 126.9, 127.8, 128.3, 128.4, 128.9, 129.4, 138.7, 139.3, 140.0, 141.1, 168.3. HR-MS *m/z* calcd for $C_{35}H_{38}N_2O_2$ $[(M + H)]^+$: 531.3001; found 531.2994.

6.1.5.35. (S)-Methyl 3-((N-benzyl-2-((tert-butoxycarbonyl)amino) pent-4-ynamido)methyl)-1-methyl-1H-indole-5-carboxylate (35). Final compound **35** was obtained following general procedure **A**, using as starting materials intermediate **33** and Boc-L-Pra-OH. FC in dichloromethane/methanol 4.8/0.2. Rf = 0.3. White powder (80% yield). ^{1}H NMR (400 MHz, CD_3OD): δ: 1.34 (s, 9H, CH_3); 2.59–2.68 (m, 3H, CH_2 and CH); 3.79 (s, 3H, CH_3); 3.92 (s, 3H, CH_3); 4.51–4.63 (m, 4H CH_2); 5.06 (t, 1H, CH, J = 6.5 Hz); 7.19–7.44 (m, 5H, aryl); 7.88 (t, 2H, aryl, J = 7.1 Hz); 8.21 (s, 1H, aryl); 8.29 (s, 1H, aryl). ^{13}C NMR (100 MHz, CD_3OD) δ 22.0, 27.2, 31.61, 31.74, 39.2, 42.1, 49.2, 49.9, 51.0, 79.3, 111.1, 120.8, 121.1, 122.1, 122.6, 126.8, 127.2, 128.1, 128.4, 130.0, 130.8, 136.4, 136.9, 139.8, 155.8, 168.5, 171.4. HR-MS *m/z* calcd for $C_{29}H_{33}N_3O_5$ $[(M + H)]^+$: 504.2493; found 504.2501.

6.1.6. Enzymatic assays

6.1.6.1. M^{pro} enzymatic assay. The assay was performed in a volume of 25 μL in black 384-well OptiPlate. A fluorescent FRET substrate (DABCYL-KTSAVLQSGFRKME-EDANS) harboring the cleavage site of SARS-COV-2 M^{pro} and aqueous buffer solution (40 mM Tris-HCl, pH 8.0, 110 mM NaCl, 2.2 mM KCl, 20% glycerol, 3 mM DTT, 8 mM maltose) were used for the inhibition assay (BPS Bioscience 3CL Protease, MBP-tagged Assay). M^{pro} recombinant protease, at a final concentration of 150 ng per reaction, was preincubated for 30 min at room temperature with the compounds at different concentrations. Finally, the reaction was initiated by adding 5 μl of the FRET substrate to each well (final concentration, 50 μM). Buffer with the same amount of DMSO (1%) was used as control and M^{pro} inhibitor GC376 is also included as a positive control. The plate was covered with a TopSeal™-A PLUS sealing film to prevent contamination and evaporation of the samples and incubated for 4 h at room temperature in subdued light.

The fluorescence signals (excitation/emission, 360 nm/460 nm) of released EDANS were read using a PerkinElmer EnSight multimode plate reader. The experiments were performed in triplicate. The IC_{50} values were calculated using GraphPad Prism 8.0 software by nonlinear regression of dose-response inhibition.

6.1.6.2. PL^{pro} enzymatic assay. The assay was performed in a volume of 50 μL in black 96-well OptiPlate. A fluorometric peptide Z-Arg-Leu-Arg-Gly-Gly-AMC (Z-RLRGG-AMC) was used as substrate in PL^{pro} enzymatic assay (BPS Bioscience Papain-like Protease Assay: Deubiquitinase Activity). Upon cleavage by PL^{pro}, the fluorescence of the AMC moiety dramatically raises. For steady state measurement, the enzyme was incubated for 30 min at 37 °C (final concentration, 25 ng per reaction) with the compounds at different concentrations in assay buffer (40 mM Tris-HCl, pH 8, 110 mM NaCl, 2.2 mM KCl, 0.04% Tween-20, 3 mM DTT, 20% glycerol and 115 mM Imidazole). Then, the reaction was initiated by adding 10 μl of the substrate to each well (final concentration, 250 nM). Buffer with the same amount of DMSO (1%) was used as control and PL^{pro} inhibitor GRL0617 is also included as a positive control. The plate was covered with a TopSeal™-A PLUS sealing film to prevent contamination and evaporation of the samples and incubated in the dark for 50 min at 37 °C. The fluorescence signals (excitation/emission, 360 nm/460 nm) were read using a PerkinElmer EnSight multimode plate reader. The experiments were performed in triplicate. The IC_{50} values were calculated using GraphPad Prism 8.0 software by nonlinear regression of dose-response inhibition.

6.1.7. SPR binding assay

SARS-Cov-2 Spike protein (SP) was acquired by Genscript Biotech, NE (cat. no. Z03501-1). Series S Sensor Chip CM5 8 (cat. no. BR100530), His Capture Kit (cat. no. 28995056), Amine Coupling Kit (cat. no. BR100050), HBS-P (cat. no. BR100368) were purchased from Cytiva.

The affinity of synthetic compounds for SARS-Cov-2 Spike protein (SP) was determined by SPR using a Biacore T200 (Cytiva) optical biosensor equipped with research-grade CM5 (Carboxy Methyl Dextran) sensor chip. Prior to the immobilization of the SP protein, a pH scouting was performed as follows. Solutions of 1.25 μM of the ligand in 10 mM sodium acetate with pH values ranging from 4.47 to 6 were prepared and injected onto the surface. The SP protein (1.25 μM in 10 mM sodium acetate, pH 4.59) was immobilized by using standard amine-coupling protocol to obtain densities of 11500 RU. HBS-P buffer (0.01 M HEPES pH 7.4, 0.15 M NaCl, 0.005% (v/v) Surfactant P20) diluted 10 × with Milli-Q water and supplemented with 5% DMSO was used as a running buffer. Stock solutions of compounds in 100% DMSO were prepared (10 mM). Running buffer was injected at a flow rate of 10 μL/min over the chip to clean and equilibrate the immobilizes sensor surface, then a solvent correction was performed as indicated in Laboratory Guideline 29-0057-18 AA, GE Healthcare Life Sciences. A series of increasing concentrations of compounds (0.75–100 μM) diluted in the ligand buffer were injected at 25 °C with a flow rate of 20 μL/min for 90s (association phase), and then the buffer alone was injected for 600 s (dissociation phase). A regeneration step was not necessary. The first channel was used as a reference surface. The experiments were performed in triplicate. The equilibrium dissociation constants (K_D) and kinetic dissociation (k_d) and association (k_a) constants were calculated from the sensorgrams by global fitting of a 1:1 binding model using evaluation software (v3.1) provided with the Biacore T200 instrument (Cytiva).

6.1.8. Cellular assay

SARS-CoV-2 antiviral assay Vero cells (ATCC-CCL81) were grown in Dulbecco's Modified Eagle's Medium (DMEM, ThermoFisher, Belgium) supplemented with 10% fetal calf serum (FCS), 2 mM L-glutamine, 0.1 mM non-essential amino acids, 1 mM sodium pyruvate, and 10 mM HEPES at 37 °C in a 5% CO_2 humidified atmosphere. The SARS-CoV-2 strains UC-1074 and UC-1075 were isolated from the nasopharyngeal swabs of two COVID-19 patients that had a Ct of 19 and 22, respectively, for the detection of the SARS-CoV-2 E protein by real-time reverse transcription PCR (RT-qPCR). The infectious virus titer of the clinical isolates was determined in Vero cells and expressed as 50% cell culture infectious dose ($CCID_{50}$) per mL. The titers of the viral stocks were 1.58E+06 (UC-1074) and 1.08E+04 (UC-1075) TCID50/mL. For the antiviral assays, Vero cells were seeded in 96-well plates at a density of 1×10^4 cells per well in DMEM 10% FCS medium. After 24 h growth, the medium was removed, and cells were treated with different compound concentrations in DMEM 2% FCS and mocked-infected or SARS-CoV-2-infected with 100 $CCID_{50}$/well (final volume 200 μl/450 well). After 5 days of incubation at 37 °C, viral CPE was recorded microscopically and the 50% effective concentration (EC_{50}) was calculated for each compound and remdesivir (reference anti-SARS-CoV-2 compound). In parallel, the cytotoxic effects of the compounds were assessed by evaluating the MCC (minimum cytotoxic concentration that causes a microscopically detectable alteration of cell morphology). The effects of the compounds on cell growth were determined by counting the number of cells with a Coulter counter in mock-infected cultures and expressed as the cytostatic concentration required to reduce cell growth by 50% (CC_{50}). All SARS-CoV-2-related work was conducted in the high-containment BSL3 facilities of the KU Leuven Rega Institute

(3CAPS) under licenses AMV 30112018 SBB 219 2018 0892 and AMV 23102017 SBB 219 2017 0589 according to institutional guidelines.

6.1.9. Computational details

3D structures of SARS-CoV-2 M^{pro} in complex with **A1** antagonist (FJC) (PDB code: 6M0K) [33] and of SARS-CoV-2 PL^{pro} in complex with non-covalent inhibitor VBY (PDB code: 7JIW) [40] and with covalent peptidic inhibitor VIR251 (PDB code: 6WX4) [24], and of SARS-CoV-2 spike protein (PDB code: 6LZG) [41] were prepared using the Schrödinger Protein Preparation Wizard workflow [55]. Specifically, water molecules and the co-complexed compounds/counterparts (ACE2 in the case of spike protein) were deleted, cap termini were included, all hydrogen atoms were added, and bond orders were assigned. Eventually, the prepared.pdb files were converted to the final.mae files. The grids accounted for the subsequent molecular docking calculations were generated analyzing the positions of the related co-crystallized compounds.

The focused library of investigated compounds (See Results and Discussion) was prepared using LigPrep software (Schrodinger Suite) [56]. Specifically, all the possible tautomers and protonation states ($pH = 7.4 \pm 1.0$) were generated for each compound, and the obtained structures were minimized using the OPLS 2005 force field.

Molecular docking experiments were performed using Glide software (Schrödinger Suite), using the Extra Precision [XP] mode [57]. In details, 20,000 poses were kept in the starting phase of docking 1200 poses for energy minimization were selected. The scoring window for keeping the initial poses was set to 400.0 and a scaling factor of 0.8 related to van der Waals radii with a partial charge cutoff of 0.15, basing on a 0.5 kcal/mol rejection cutoff for the obtained minimized poses, was considered. In the output file, 10 poses for each compound were saved.

Covalent docking experiments were performed using Glide software (Schrödinger Suite) [57]. Cys145 was set as the reactive protein residue for SARS-CoV-2 M^{pro} and Cys111 for SARS-CoV-2 PL^{pro}, whereas the specific reaction type was selected in the related panel according to the specific ligand chemical features. When needed, the specific.cdock "custom chemistry" file was generated. In the output file, 10 poses for each compound were saved.

Funding

This research did not receive any specific grant from funding agencies in the public, commercial, or not-for-profit sectors.

Declaration of competing interest

The authors declare that they have no known competing financial interests or personal relationships that could have appeared to influence the work reported in this paper.

Acknowledgements

The authors are grateful to M Brecht Dirix for excellent technical assistance in the biological assays.

Appendix A. Supplementary data

Supplementary data to this article can be found online at https://doi.org/10.1016/j.ejmech.2021.113863.

References

[1] K. Dhama, S.K. Patel, K. Sharun, M. Pathak, R. Tiwari, M.I. Yatoo, Y.S. Malik, R. Sah, A.A. Rabaan, P.K. Panwar, K.P. Singh, I. Michalak, W. Chaicumpa, D.F. Martinez-Pulgarin, D.K. Bonilla-Aldana, A.J. Rodriguez-Morales, SARS-CoV-2 jumping the species barrier: zoonotic lessons from SARS, MERS and recent advances to combat this pandemic virus, Trav. Med. Infect. Dis. 37 (2020) 101830.

[2] R. Tiwari, K. Dhama, K. Sharun, M. Iqbal Yatoo, Y.S. Malik, R. Singh, I. Michalak, R. Sah, D.K. Bonilla-Aldana, A.J. Rodriguez-Morales, COVID-19: animals, veterinary and zoonotic links, Vet. Q. 40 (2020) 169–182.

[3] J.R. Larsen, M.R. Martin, J.D. Martin, P. Kuhn, J.B. Hicks, Modeling the onset of symptoms of COVID-19, Front Public Health 8 (2020) 473.

[4] C.R. Triggle, D. Bansal, H. Ding, M.M. Islam, E. Farag, H.A. Hadi, A.A. Sultan, A comprehensive review of viral characteristics, transmission, pathophysiology, immune response, and management of SARS-CoV-2 and COVID-19 as a basis for controlling the pandemic, Front. Immunol. 12 (2021) 631139.

[5] S. Falahi, A. Kenarkoohi, Transmission routes for SARS-CoV-2 infection: review of evidence, New Microbes New Infect 38 (2020) 100778.

[6] E.e. team, Updated rapid risk assessment from ECDC on the risk related to the spread of new SARS-CoV-2 variants of concern in the EU/EEA – first update, Euro Surveill. 26 (2021) 2101211.

[7] R.T. Eastman, J.S. Roth, K.R. Brimacombe, A. Simeonov, M. Shen, S. Patnaik, M.D. Hall, Remdesivir: a review of its discovery and development leading to emergency use authorization for treatment of COVID-19, ACS Cent. Sci. 6 (2020) 672–683.

[8] Y. Wang, D. Zhang, G. Du, R. Du, J. Zhao, Y. Jin, S. Fu, L. Gao, Z. Cheng, Q. Lu, Y. Hu, G. Luo, K. Wang, Y. Lu, H. Li, S. Wang, S. Ruan, C. Yang, C. Mei, Y. Wang, D. Ding, F. Wu, X. Tang, X. Ye, Y. Ye, B. Liu, J. Yang, W. Yin, A. Wang, G. Fan, F. Zhou, Z. Liu, X. Gu, J. Xu, L. Shang, Y. Zhang, L. Cao, T. Guo, Y. Wan, H. Qin, Y. Jiang, T. Jaki, F.G. Hayden, P.W. Horby, B. Cao, C. Wang, Remdesivir in adults with severe COVID-19: a randomised, double-blind, placebo-controlled, multicentre trial, Lancet 395 (2020) 1569–1578.

[9] H.M. Dabbous, S. Abd-Elsalam, M.H. El-Sayed, A.F. Sherief, F.F.S. Ebeid, M.S.A. El Ghafar, S. Soliman, M. Elbahnasawy, R. Badawi, M.A. Tageldin, Efficacy of favipiravir in COVID-19 treatment: a multi-center randomized study, Arch. Virol. 166 (2021) 949–954.

[10] D. Bojkova, M. Bechtel, K.M. McLaughlin, J.E. McGreig, K. Klann, C. Bellinghausen, G. Rohde, D. Jonigk, P. Braubach, S. Ciesek, C. Munch, M.N. Wass, M. Michaelis, J. Cinatl Jr., Aprotinin inhibits SARS-CoV-2 replication, Cells 9 (2020).

[11] O.J. McElvaney, E. O'Connor, N.L. McEvoy, D.D. Fraughan, J. Clarke, O.F. McElvaney, C. Gunaratnam, J. O'Rourke, G.F. Curley, N.G. McElvaney, Alpha-1 antitrypsin for cystic fibrosis complicated by severe cytokinemic COVID-19, J. Cyst. Fibros. 20 (2021) 31–35.

[12] J.M. Grimes, K.V. Grimes, p38 MAPK inhibition: a promising therapeutic approach for COVID-19, J. Mol. Cell. Cardiol. 144 (2020) 63–65.

[13] R. Covid, C. Treatments, Use of hydroxychloroquine in hospitalised COVID-19 patients is associated with reduced mortality: findings from the observational multicentre Italian CORIST study, Eur. J. Intern. Med. 82 (2020) 38–47.

[14] S.A. Meo, D.C. Klonoff, J. Akram, Efficacy of chloroquine and hydroxychloroquine in the treatment of COVID-19, Eur. Rev. Med. Pharmacol. Sci. 24 (2020) 4539–4547.

[15] X. Ou, Y. Liu, X. Lei, P. Li, D. Mi, L. Ren, L. Guo, R. Guo, T. Chen, J. Hu, Z. Xiang, Z. Mu, X. Chen, J. Chen, K. Hu, Q. Jin, J. Wang, Z. Qian, Characterization of spike glycoprotein of SARS-CoV-2 on virus entry and its immune cross-reactivity with SARS-CoV, Nat. Commun. 11 (2020) 1620.

[16] Y. Xie, C.B. Karki, D. Du, H. Li, J. Wang, A. Sobitan, S. Teng, Q. Tang, L. Li, Spike proteins of SARS-CoV and SARS-CoV-2 utilize different mechanisms to bind with human ACE2, Front Mol Biosci 7 (2020) 591873.

[17] S. Di Micco, S. Musella, M.C. Scala, M. Sala, P. Campiglia, G. Bifulco, A. Fasano, In silico analysis revealed potential anti-SARS-CoV-2 main protease activity by the zonulin inhibitor larazotide acetate, Front Chem 8 (2021) 628609.

[18] J. Sultana, S. Crisafulli, F. Gabbay, E. Lynn, S. Shakir, G. Trifirò, Challenges for drug repurposing in the COVID-19 pandemic era, Front. Pharmacol. 11 (2020) 1657.

[19] Y. Huang, C. Yang, X.F. Xu, W. Xu, S.W. Liu, Structural and functional properties of SARS-CoV-2 spike protein: potential antivirus drug development for COVID-19, Acta Pharmacol. Sin. 41 (2020) 1141–1149.

[20] FDA's Approval of Veklury (Remdesivir) for the Treatment of COVID-19—The Science of Safety and Effectiveness. https://www.fda.gov/drugs/drug-safety-and-availability/fdas-approval-veklury-remdesivir-treatment-covid-19-science-safety-and-effectiveness lastly accessed 07/19/2021.

[21] G. Kokic, H.S. Hillen, D. Tegunov, C. Dienemann, F. Seitz, J. Schmitzova, L. Farnung, A. Siewert, C. Hobartner, P. Cramer, Mechanism of SARS-CoV-2 polymerase stalling by remdesivir, Nat. Commun. 12 (2021) 279.

[22] M. Gioia, C. Ciaccio, P. Calligari, G. De Simone, D. Sbardella, G. Tundo, G.F. Fasciglione, A. Di Masi, D. Di Pierro, A. Bocedi, P. Ascenzi, M. Coletta, Role of proteolytic enzymes in the COVID-19 infection and promising therapeutic approaches, Biochem. Pharmacol. 182 (2020) 114225.

[23] Q. Li, C. Kang, Progress in developing inhibitors of SARS-CoV-2 3C-like protease, Microorganisms 8 (2020) 1250.

[24] W. Rut, Z. Lv, M. Zmudzinski, S. Patchett, D. Nayak, S.J. Snipas, F. El Oualid, T.T. Huang, M. Bekes, M. Drag, S.K. Olsen, Activity profiling and crystal

structures of inhibitor-bound SARS-CoV-2 papain-like protease: a framework for anti-COVID-19 drug design, Sci Adv 6 (2020), eabd4596.
[25] D. Zaidman, P. Gehrtz, M. Filep, D. Fearon, J. Prilusky, S. Duberstein, G. Cohen, D. Owen, E. Resnick, C. Strain-Damerell, P. Lukacik, H. Barr, M.A. Walsh, F. von Delft, N. London, An Automatic Pipeline for the Design of Irreversible Derivatives Identifies a Potent SARS-CoV-2 M^{pro} Inhibitor, bioRxiv, 2020, 2020.2009.2021.299776.
[26] K. Arafet, N. Serrano-Aparicio, A. Lodola, A.J. Mulholland, F.V. González, K. Świderek, V. Moliner, Mechanism of inhibition of SARS-CoV-2 Mpro by N3 peptidyl Michael acceptor explained by QM/MM simulations and design of new derivatives with tunable chemical reactivity, Chem. Sci. 12 (2021) 1433–1444.
[27] A.S. Paul, R. Islam, M.R. Parves, A.A. Mamun, I. Shahriar, M.I. Hossain, M.N. Hossain, M.A. Ali, M.A. Halim, Cysteine focused covalent inhibitors against the main protease of SARS-CoV-2, J. Biomol. Struct. Dyn. (2020) 1–20.
[28] R.L. Hoffman, R.S. Kania, M.A. Brothers, J.F. Davies, R.A. Ferre, K.S. Gajiwala, M. He, R.J. Hogan, K. Kozminski, L.Y. Li, J.W. Lockner, J. Lou, M.T. Marra, L.J. Mitchell Jr., B.W. Murray, J.A. Nieman, S. Noell, S.P. Planken, T. Rowe, K. Ryan, G.J. Smith 3rd, J.E. Solowiej, C.M. Steppan, B. Taggart, Discovery of ketone-based covalent inhibitors of coronavirus 3CL proteases for the potential therapeutic treatment of COVID-19, J. Med. Chem. 63 (2020) 12725–12747.
[29] G.J. Lockbaum, A.C. Reyes, J.M. Lee, R. Tilvawala, E.A. Nalivaika, A. Ali, N. Kurt Yilmaz, P.R. Thompson, C.A. Schiffer, Crystal structure of SARS-CoV-2 main protease in complex with the non-covalent inhibitor ML188, Viruses 13 (2021) 174.
[30] C.H. Zhang, E.A. Stone, M. Deshmukh, J.A. Ippolito, M.M. Ghahremanpour, J. Tirado-Rives, K.A. Spasov, S. Zhang, Y. Takeo, S.N. Kudalkar, Z. Liang, F. Isaacs, B. Lindenbach, S.J. Miller, K.S. Anderson, W.L. Jorgensen, Potent noncovalent inhibitors of the main protease of SARS-CoV-2 from molecular sculpting of the drug perampanel guided by free energy perturbation calculations, ACS Cent. Sci. 7 (2021) 467–475.
[31] N. Kitamura, M.D. Sacco, C. Ma, Y. Hu, J.A. Townsend, X. Meng, F. Zhang, X. Zhang, M. Ba, T. Szeto, A. Kukuljac, M.T. Marty, D. Schultz, S. Cherry, Y. Xiang, Y. Chen, J. Wang, Expedited approach toward the rational design of noncovalent SARS-CoV-2 main protease inhibitors, J. Med. Chem. (2021), https://doi.org/10.1021/acs.jmedchem.1c00509.
[32] C. Ostacolo, V. Di Sarno, G. Lauro, G. Pepe, S. Musella, T. Ciaglia, V. Vestuto, G. Autore, G. Bifulco, S. Marzocco, P. Campiglia, I.M. Gomez-Monterrey, A. Bertamino, Identification of an indol-based multi-target kinase inhibitor through phenotype screening and target fishing using inverse virtual screening approach, Eur. J. Med. Chem. 167 (2019) 61–75.
[33] W. Dai, B. Zhang, X.M. Jiang, H. Su, J. Li, Y. Zhao, X. Xie, Z. Jin, J. Peng, F. Liu, C. Li, Y. Li, F. Bai, H. Wang, X. Cheng, X. Cen, S. Hu, X. Yang, J. Wang, X. Liu, G. Xiao, H. Jiang, Z. Rao, L.K. Zhang, Y. Xu, H. Yang, H. Liu, Structure-based design of antiviral drug candidates targeting the SARS-CoV-2 main protease, Science 368 (2020) 1331–1335.
[34] H. Yang, W. Xie, X. Xue, K. Yang, J. Ma, W. Liang, Q. Zhao, Z. Zhou, D. Pei, J. Ziebuhr, R. Hilgenfeld, K.Y. Yuen, L. Wong, G. Gao, S. Chen, Z. Chen, D. Ma, M. Bartlam, Z. Rao, Design of wide-spectrum inhibitors targeting coronavirus main proteases, PLoS Biol. 3 (2005) e324.
[35] H. Kim, Y.S. Hwang, M. Kim, S.B. Park, Recent advances in the development of covalent inhibitors, Rsc Med Chem 12 (2021) 1037–1045.
[36] E. Mons, I.D.C. Jansen, J. Loboda, B.R. van Doodewaerd, J. Hermans, M. Verdoes, C.A.A. van Boeckel, P.A. van Veelen, B. Turk, D. Turk, H. Ovaa, The alkyne moiety as a latent electrophile in irreversible covalent small molecule inhibitors of cathepsin K, J. Am. Chem. Soc. 141 (2019) 3507–3514.
[37] S. Sommer, N.D. Weikart, U. Linne, H.D. Mootz, Covalent inhibition of SUMO and ubiquitin-specific cysteine proteases by an in situ thiol-alkyne addition, Bioorg. Med. Chem. 21 (2013) 2511–2517.
[38] S. Krishnan, R.M. Miller, B. Tian, R.D. Mullins, M.P. Jacobson, J. Taunton, Design of reversible, cysteine-targeted Michael acceptors guided by kinetic and computational analysis, J. Am. Chem. Soc. 136 (2014) 12624–12630.
[39] C. Locatelli, R. Rosso, M.C. Santos-Silva, C.A. de Souza, M.A. Licínio, P. Leal, M.L. Bazzo, R.A. Yunes, T.B. Creczynski–Pasa, Ester derivatives of gallic acid with potential toxicity toward L1210 leukemia cells, Bioorg. Med. Chem. 16 (2008) 3791–3799.
[40] T.T. Liao, L. Wang, R.W. Jia, X.H. Fu, H. Chua, Lipophilic organic pollutants induce changes in phospholipid and membrane protein composition leading to Vero cell morphological change, J Environ Sci Heal B 49 (2014) 760–768.
[41] J. Osipiuk, S.A. Azizi, S. Dvorkin, M. Endres, R. Jedrzejczak, K.A. Jones, S. Kang, R.S. Kathayat, Y. Kim, V.G. Lisnyak, S.L. Maki, V. Nicolaescu, C.A. Taylor, C. Tesar, Y.A. Zhang, Z. Zhou, G. Randall, K. Michalska, S.A. Snyder, B.C. Dickinson, A. Joachimiak, Structure of papain-like protease from SARS-CoV-2 and its complexes with non-covalent inhibitors, Nat. Commun. 12 (2021) 743.
[42] Q. Wang, Y. Zhang, L. Wu, S. Niu, C. Song, Z. Zhang, G. Lu, C. Qiao, Y. Hu, K.-Y. Yuen, Q. Wang, H. Zhou, J. Yan, J. Qi, Structural and functional basis of SARS-CoV-2 entry by using human ACE2, Cell 181 (2020) 894–904, e9.
[43] D.E. Gordon, G.M. Jang, M. Bouhaddou, J. Xu, K. Obernier, K.M. White, M.J. O'Meara, V.V. Rezelj, J.Z. Guo, D.L. Swaney, T.A. Tummino, R. Huttenhain, R.M. Kaake, A.L. Richards, B. Tutuncuoglu, H. Foussard, J. Batra, K. Haas, M. Modak, M. Kim, P. Haas, B.J. Polacco, H. Braberg, J.M. Fabius, M. Eckhardt, M. Soucheray, M.J. Bennett, M. Cakir, M.J. McGregor, Q. Li, B. Meyer, F. Roesch, T. Vallet, A. Mac Kain, L. Miorin, E. Moreno, Z.Z.C. Naing, Y. Zhou, S. Peng, Y. Shi, Z. Zhang, W. Shen, I.T. Kirby, J.E. Melnyk, J.S. Chorba, K. Lou, S.A. Dai, I. Barrio-Hernandez, D. Memon, C. Hernandez-Armenta, J. Lyu, C.J.P. Mathy, T. Perica, K.B. Pilla, S.J. Ganesan, D.J. Saltzberg, R. Rakesh, X. Liu, S.B. Rosenthal, L. Calviello, S. Venkataramanan, J. Liboy-Lugo, Y. Lin, X.P. Huang, Y. Liu, S.A. Wankowicz, M. Bohn, M. Safari, F.S. Ugur, C. Koh, N.S. Savar, Q.D. Tran, D. Shengjuler, S.J. Fletcher, M.C. O'Neal, Y. Cai, J.C.J. Chang, D.J. Broadhurst, S. Klippsten, P.P. Sharp, N.A. Wenzell, D. Kuzuoglu-Ozturk, H.Y. Wang, R. Trenker, J.M. Young, D.A. Cavero, J. Hiatt, T.L. Roth, U. Rathore, A. Subramanian, J. Noack, M. Hubert, R.M. Stroud, A.D. Frankel, O.S. Rosenberg, K.A. Verba, D.A. Agard, M. Ott, M. Emerman, N. Jura, M. von Zastrow, E. Verdin, A. Ashworth, O. Schwartz, C. d'Enfert, S. Mukherjee, M. Jacobson, H.S. Malik, D.G. Fujimori, T. Ideker, C.S. Craik, S.N. Floor, J.S. Fraser, J.D. Gross, A. Sali, B.L. Roth, D. Ruggero, J. Taunton, T. Kortemme, P. Beltrao, M. Vignuzzi, A. Garcia-Sastre, K.M. Shokat, B.K. Shoichet, N.J. Krogan, A SARS-CoV-2 protein interaction map reveals targets for drug repurposing, Nature 583 (2020) 459–468.
[44] S. Sadegh, J. Matschinske, D.B. Blumenthal, G. Galindez, T. Kacprowski, M. List, R. Nasirigerdeh, M. Oubounyt, A. Pichlmair, T.D. Rose, M. Salgado-Albarran, J. Spath, A. Stukalov, N.K. Wenke, K. Yuan, J.K. Pauling, J. Baumbach, Exploring the SARS-CoV-2 virus-host-drug interactome for drug repurposing, Nat. Commun. 11 (2020) 3518.
[45] Y. Zhou, Y. Hou, J. Shen, Y. Huang, W. Martin, F. Cheng, Network-based drug repurposing for novel coronavirus 2019-nCoV/SARS-CoV-2, Cell Discov 6 (2020) 14.
[46] A. Sternberg, D.L. McKee, C. Naujokat, Novel drugs targeting the SARS-CoV-2/COVID-19 machinery, Curr. Top. Med. Chem. 20 (2020) 1423–1433.
[47] K. Mitra, P. Ghanta, S. Acharya, G. Chakrapani, B. Ramaiah, M. Doble, Dual inhibitors of SARS-CoV-2 proteases: pharmacophore and molecular dynamics based drug repositioning and phytochemical leads, J. Biomol. Struct. Dyn. (2020) 1–14.
[48] S. Rajpoot, M. Alagumuthu, M.S. Baig, Dual targeting of 3CLpro and PLpro of SARS-CoV-2: a novel structure-based design approach to treat COVID-19, Curr Res Struct Biol 3 (2021) 9–18.
[49] K. Baby, S. Maity, C.H. Mehta, A. Suresh, U.Y. Nayak, Y. Nayak, SARS-CoV-2 entry inhibitors by dual targeting TMPRSS2 and ACE2: an in silico drug repurposing study, Eur. J. Pharmacol. 896 (2021) 173922.
[50] B. Naik, N. Gupta, R. Ojha, S. Singh, V.K. Prajapati, D. Prusty, High throughput virtual screening reveals SARS-CoV-2 multi-target binding natural compounds to lead instant therapy for COVID-19 treatment, Int. J. Biol. Macromol. 160 (2020) 1–17.
[51] M. Zmudzinski, W. Rut, K. Olech, J. Granda, M. Giurg, M. Burda-Grabowska, L. Zhang, X. Sun, Z. Lv, D. Nayak, M. Kesik-Brodacka, S.K. Olsen, R. Hilgenfeld, M. Drag, Ebselen Derivatives Are Very Potent Dual Inhibitors of SARS-CoV-2 Proteases - PL^{pro} and M^{pro} in in Vitro Studies, bioRxiv, 2020, 2020.2008.2030.273979.
[52] Z. Chen, Q. Cui, L. Cooper, P. Zhang, H. Lee, Z. Chen, Y. Wang, X. Liu, L. Rong, R. Du, Ginkgolic acid and anacardic acid are specific covalent inhibitors of SARS-CoV-2 cysteine proteases, Cell Biosci. 11 (2021) 45.
[53] C. Ma, Y. Hu, J.A. Townsend, P.I. Lagarias, M.T. Marty, A. Kolocouris, J. Wang, Ebselen, disulfiram, carmofur, PX-12, tideglusib, and shikonin are nonspecific promiscuous SARS-CoV-2 main protease inhibitors, ACS Pharmacol Transl Sci 3 (2020) 1265–1277.
[54] P.A. Temussi, M. Grimaldi, I. Stillitano, G. Amodio, A. Santoro, M. Buonocore, O. Moltedo, P. Remondelli, A.M. D'Ursi, Structural basis of antiviral activity of peptides from MPER of FIV gp36, PloS One 13 (2018), e0204042.
[55] Schrödinger Release 2021-2: Protein Preparation Wizard, Epik, Schrödinger, LLC, New York, NY, 2021. Impact, Schrödinger, LLC, New York, NY; Prime, Schrödinger, LLC, New York, NY, 2021.
[56] Schrödinger Release 2021-2, LigPrep, Schrödinger, LLC, New York, NY, 2021.
[57] Schrödinger Release 2021-2: Glide, Schrödinger, LLC, New York, NY, 2021.